JACK N. AVERITT COLLEGE of GRADUATE STUDIES GEORGIA SOUTHERN UNIVERSITY

Georgia Southern University

Digital Commons@Georgia Southern

Electronic Theses and Dissertations

Graduate Studies, Jack N. Averitt College of

Fall 2014

Computational and Experimental Study on Vertical Axis Wind Turbine in Search for an Efficient Design

Mohammad M. Bashar

Follow this and additional works at: https://digitalcommons.georgiasouthern.edu/etd

Part of the Computer-Aided Engineering and Design Commons, Energy Systems Commons, and the Other Mechanical Engineering Commons

Recommended Citation

Bashar, Mohammad M., "Computational and Experimental Study on Vertical Axis Wind Turbine in Search for an Efficient Design" (2014). *Electronic Theses and Dissertations*. 1184.
https://digitalcommons.georgiasouthern.edu/etd/1184

This thesis (open access) is brought to you for free and open access by the Graduate Studies, Jack N. Averitt College of at Digital Commons@Georgia Southern. It has been accepted for inclusion in Electronic Theses and Dissertations by an authorized administrator of Digital Commons@Georgia Southern. For more information, please contact digitalcommons@georgiasouthern.edu.

COMPUTATIONAL AND EXPERIMENTAL STUDY ON VERTICAL AXIS WIND TURBINE IN SEARCH FOR AN EFFICIENT DESIGN

by

MOHAMMAD MOHIBBUL BASHAR

(Under the Direction of Mosfequr Rahman)

ABSTRACT

Wind alone can fulfill most of the energy requirement of the world by its efficient conversion in to energy. Though Horizontal Axis Wind Turbine (HAWT) is more popular but needs high wind speed to generate energy. On the other hand Vertical Axis Wind Turbine (VAWT) needs low wind speed and can be installed anywhere which are some of the reasons for this research. The main objective of this research is to improve the design and performance of VAWT to make it more attractive, efficient, durable and sustainable. For a VAWT the blades perform the main role to extract energy from the wind. Airfoil is considered as the blade for this new design of VAWT. Airfoil has some good aerodynamic characteristics, match with the characteristics of Savonius type VAWT, such as good stall characteristics and little roughness effect, relatively high drag and low lift coefficient. Integration of Computational Fluid Dynamics (CFD) simulation and wind tunnel experimentation has made the current research more acceptable. 3-Dimensional CAD models of various simple airfoils have been designed in Solidworks. Using these airfoils and other shape, CFD simulation has been performed with five different VAWT designed models. Moving mesh and fluid flow simulation have been developed in CFD software FLUENT. The findings of these numerical simulations provided pressure contour, velocity contour, drag coefficient, lift coefficient,

torque coefficient and power coefficient for all these models. Physical models of NACA5510, NACA7510 and semicircular rotors of three bladed are fabricated and tested in-house subsonic wind tunnel. From these experiments dynamic torque has been measured using dynamic torque sensors for all these models at three different speeds. By comparing the numerical and experimental results it can be concluded that NACA7510 air foiled VAWT model gives the better performance at higher Tip Speed Ratio than other two models.

Keywords: wind energy, vertical axis wind turbine, renewable energy, clean electricity, Savonius Turbine, CFD.

COMPUTATIONAL AND EXPERIMENTAL STUDY ON VERTICAL AXIS WIND TURBINE IN SEARCH FOR AN EFFICIENT DESIGN

by

MOHAMMAD MOHIBBUL BASHAR

B.Sc. (Eng.) in Mechanical Engineering, Bangladesh University of Engineering and Technology, Bangladesh 2005

MBA in Finance, Dhaka University, Bangladesh 2011

A Thesis Submitted to the Graduate Faculty of the Georgia Southern University

in Partial Fulfillment of the Requirement of the Degree of

MASTERS OF SCIENCE IN APPLIED ENGINEERING

in

Mechanical Engineering

Georgia Southern University

Statesboro, Georgia

© 2014

MOHAMMAD MOHIBBUL BASHAR

All Rights Reserved

COMPUTATIONAL AND EXPERIMENTAL STUDY ON VERTICAL AXIS WIND TURBINE IN SEARCH FOR AN EFFICIENT DESIGN

by

MOHAMMAD MOHIBBUL BASHAR

Major Professor:	Mosfequr Rahman
Committee:	Aniruddha Mitra
	Cheng Zhang

Electronic Version Approved:
December 2014

DEDICATION

To my family who have been always

beside me to work hard and pursue my goals.

ACKNOWLEDGEMENTS

My sincere gratitude is for my Research advisor Dr. Mosfequr Rahman for his valuable guidance, direction and encouragement throughout the progress of this research at Georgia Southern University and his precious time to pursue the goals. I would like to express my gratitude to Dr. Aniruddha Mitra and Dr. Cheng Zhang for their kind participation as members of my supervisory committee.

I am grateful to all of those with whom I have had the pleasure to work during this and other related projects. Dr. Jobaidur Khan who has taught me more than I could ever give him credit for here.

I wish to thank Dr. Khandakar N Morshed for always guiding me in many discussions and providing invaluable pieces of advice. Special gratitude is for Mr. Aktaruzzaman for his enormous support during the experimental setup.

Finally I wish to thank Mr. Andrew Michaud and Mr. Saheem Absar for their help.

TABLE OF CONTENTS

ACKNOWLEDGEMENTS VII

LIST OF FIGURES X

LIST OF TABLES XIII

LIST OF SYMBOLS XIV

CHAPTER 1 1

1 INTRODUCTION 1

1.1 Alternative Energy 1

1.2 Wind Energy 2

1.3 Wind Turbine and Types 2

1.4 Vertical Axis Wind Turbines 4

1.5 Wind Energy Utilization 5

1.6 Motivation of Research 7

1.7 Scope of Research 7

1.8 Objectives of the Research 8

1.9 Outline of the Thesis 9

CHAPTER 2 10

2 LITERATURE REVIEW 10

2.1 Introduction 10

2.2 History of Wind Turbine 10

2.3 Review on Savonius Rotor 12

2.4 Review on Darrieus Rotor *16*

2.5 Review on Hybrid Rotor *19*

CHAPTER 3 ..... **20**

3 METHODOLOGY 20

3.1 Experimental Design *21*

3.2 Mathematical Relations *22*

3.3 Numerical Method *24*

3.4 Experimental Method *30*

3.5 Measured characteristics *33*

CHAPTER 4 ..... **34**

4 FINDINGS OF THE STUDY 34

4.1 Numerical Results *34*

4.2 Experimental Results *63*

4.3 Comparison of Numerical and Experimental Power Coefficient *65*

CHAPTER 5 ..... **67**

5 CONCLUSION AND RECOMMENDATION 67

5.1 Conclusion *67*

5.2 Recommendation *68*

REFERENCE **69**

LIST OF FIGURES

FIGURE 1-1: Global Renewable Power Capacity 1

FIGURE 1-2: Power Coefficient (C_p) vs. TSR (λ) For Various Wind Turbines 3

FIGURE 1-3: Global Cumulative Capacity of Wind Energy 5

FIGURE 1-4: Projected and Actual Installation of Wind Energy by DOE 6

FIGURE 1-5: Wind Energy Generation Capacity by Country 6

FIGURE 3-1: Airfoil Terminology 21

FIGURE 3-2: Schematic Diagram of the Drag Force Components on Model Cross-Section 23

FIGURE 3-3: Comparative View of NACA 5510, NACA7510 and NACA9510 24

FIGURE 3-4: Isometric View of All Five Blade Profiles 25

FIGURE 3-5: Isometric View of Models of NACA5510, NACA7510 and NACA9510 25

FIGURE 3-6: Mesh around the Airfoil Using ANSYS 26

FIGURE 3-7: Residual Convergence of Model NACA5510 at 12.5 m/s 28

FIGURE 3-8: Residual Convergence of Model NACA7510 at 10 m/s 28

FIGURE 3-9: Residual Convergence of Model NACA9510 at 15 m/s 28

FIGURE 3-10: Residual Convergence of Quarter Circular Bladed Model at 10 m/s 29

FIGURE 3-11: Residual Convergence of Semi Circular Bladed Model at 15 m/s 29

FIGURE 3-12: Complete Experimental Setup of Wind Tunnel 30

FIGURE 3-13: Fabricated Model of NACA5510 Bladed Rotor 31

FIGURE 3-14: Fabricated Model of Semi Circular Bladed Rotor 32

FIGURE 4-1: Pressure Contour around NACA5510 at Different TSR 35

FIGURE 4-2: Pressure Contour around NACA7510 at Different TSR 36

FIGURE 4-3: Pressure Contour around NACA9510 at Different TSR..... 37

FIGURE 4-4: Pressure Contour around Quarter-Circular at Different TSR 38

FIGURE 4-5: Pressure Contour around Semi-Circular Rotor at Different TSR 39

FIGURE 4-6: Velocity Contour around NACA5510 at Different TSR 41

FIGURE 4-7: Velocity Contour around NACA7510 at Different TSR 42

FIGURE 4-8 Velocity Contour around NACA9510 at Different TSR..... 43

FIGURE 4-9: Velocity Contour around Quarter-Circular at Different TSR 44

FIGURE 4-10: Velocity Contour around Semi-Circular at Different TSR 45

FIGURE 4-11: Drag Coefficient (Cd) vs. Angle of rotation (θ) for Single Blade and Three Blades Combined Effect at TSR 0.226 for Five Models..... 48

FIGURE 4-12: Drag Coefficient (Cd) vs. Angle of rotation (θ) for Three Blades Combined Effect at TSR 0.226 for Five Models 48

FIGURE 4-13: Drag Coefficient (C_d) vs. Time for NACA5510 for Different TSR 49

FIGURE 4-14: Drag Coefficient (C_d) vs. Time for NACA7510 for Different TSR 49

FIGURE 4-15: Drag Coefficient (C_d) vs. Time for NACA9510 for Different TSR 50

FIGURE 4-16: Drag Coefficient (C_d) vs. Time for Quarter-Circ. Rotor for Different TSR .. 50

FIGURE 4-17: Drag Coefficient (C_d) vs. Time for Semi-Circular rotor for Different TSR .. 51

FIGURE 4-18: Average Drag Coefficient (C_d) vs. TSR (λ) for Different Blades..... 51

FIGURE 4-19: Lift Coefficient (Cl) vs. Angle of rotation (θ) for Single Blade and..... 53

FIGURE 4-20: Lift Coefficient (Cl) vs. Angle of rotation (θ) for Three Blades Combined Effect at TSR 0.226 for Five Models 53

FIGURE 4-21: Lift Coefficient (C_l) vs. Time for NACA5510 for Different TSR..... 54

FIGURE 4-22: Lift Coefficient (C_l) vs. Time for NACA7510 for Different TSR..... 54

FIGURE 4-23: Lift Coefficient (C_l) vs. Time for NACA9510 for Different TSR 55

FIGURE 4-24: Lift Coefficient (C_l) vs. Time for Quarter-Circular Rotor for Different TSR 55

FIGURE 4-25: Lift Coefficient (C_l) vs. Time for Semi-Circular Rotor for Different TSR ... 56

FIGURE 4-26: Average Lift Coefficient (C_l) vs. TSR (λ) for Different Blades 56

FIGURE 4-27: Torque Coefficient (C_q) vs. Angle of rotation (θ) for Single Blade and Three Blades Combined Effect at TSR 0.226 for Five Models..... 58

FIGURE 4-28: Torque Coefficient (C_q) vs. Angle of rotation (θ) for Three Blades Combined Effect at TSR 0.226 for Five Models 59

FIGURE 4-29: Torque (T) at 5sec. vs. TSR (λ) for Different Blades 59

FIGURE 4-30: Calculated Torque Coefficient (C_q) vs. TSR (λ) for Different Blades..... 60

FIGURE 4-31: Computational Torque Coefficient (C_q) vs. TSR (λ) for Different Blades.... 60

FIGURE 4-32: Averaged Torque Coefficient (C_q) vs. TSR (λ) for Different Blades 61

FIGURE 4-33: Calculated Power Coefficient (C_p) at 5sec. vs. TSR (λ) for Different Blades 62

FIGURE 4-34: Computational Power Coefficient (C_p) vs. TSR (λ) for Different Blades 62

FIGURE 4-35: Averaged Power Coefficient (C_p) vs. TSR (λ) for Different Blades 63

FIGURE 4-36: Torque Coefficient (C_q) vs. TSR (λ) for Different Blades..... 64

FIGURE 4-37: Power Coefficient (C_p) vs. TSR (λ) for Different Blades 64

FIGURE 4-38: Torque Coefficient (C_q) vs. TSR (λ) of Numerical & Experimental Result. 65

FIGURE 4-39: Power Coefficient (C_p) vs. TSR (λ) of Numerical & Experimental Result ... 66

LIST OF TABLES

TABLE 1: Max and Min Pressure after 5 Sec of Rotation for All the Rotor Models at Different TSR..... 40

TABLE 2: Max and Min Velocity after 5 Sec of Rotation for All the Rotor Models at Different TSR..... 46

LIST OF SYMBOLS

Symbol	Explanation
A	Rotor Area
D	Overall Rotor Diameter
d	Blade Diameter
H	Rotor Height
V	Wind Velocity, m/s
N	Revolution per Minute
ω	Angular Velocity, rad/sec
ν	Kinematic Viscosity, m^2/s
ρ	Air Density, kg/m^3
Re	Reynolds Number
λ	Tip Speed Ratio
T	Torque
P	Power
F_l	Lift Force
F_d	Drag Force
C_d	Drag Coefficient

C_l	Lift Coefficient
C_q	Torque Coefficient
C_p	Power Coefficient

CHAPTER 1

1 Introduction

The continuous improvement of this world is based on technological advancement. And the technological advancement is directly related to the utilization of energy. The demand of energy is creeping up every day due to increase of population, industrial and agricultural advancement. But the conventional energy sources are becoming limited which is ultimately making them more expensive. In addition to this, everyone is concerned about global climate change. This whole scenario is pushing the world to find the alternative sources of energy.

1.1 Alternative Energy

Alternative sources involve natural phenomena such as sunlight, wind, tides, plant growth, and geothermal heat. Solar and Wind power are the most popular among the various sources of renewable energy. Only these two kinds of alternative sources can generate most of the world's electricity within next 50 years, on the other hand which can also help the climate change condition.

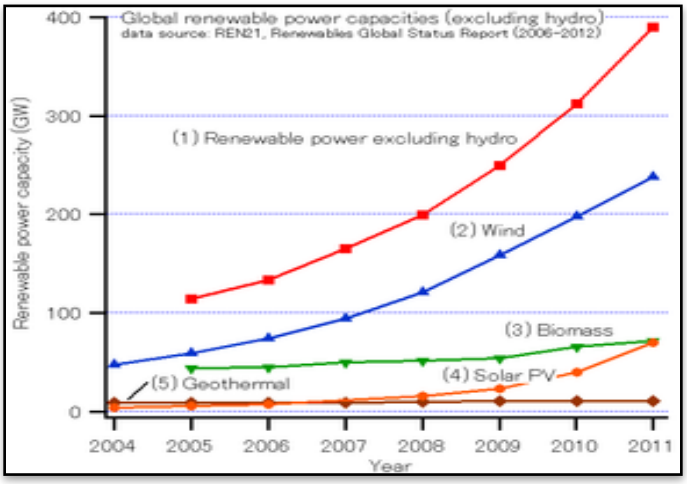

FIGURE 1-1: Global Renewable Power Capacity (REN21 2014)

1.2 Wind Energy

Wind energy has the potential to resolve the power demand of the entire world if it can be converted into electricity efficiently. Wind is going to be the most popular alternative energy source; because of its availability throughout place and time. As a pollution free and sustainable source, wind is getting importance in energy policy too. The disadvantages are its lower efficiency and high installation cost. But the ultimate cost would be lowered if it operates continuously and small scale turbines can be installed in any corner of the world.

1.3 Wind Turbine and Types

Wind turbine converts the wind energy into mechanical energy and that mechanical energy is used for the production of electricity. There are two types of primary wind turbine; they are horizontal-axis wind turbine (HAWT) and vertical-axis wind turbine (VAWT), both of which boast of being better than the other.

HAWTs include both upwind and downwind configuration with various performance enhancers such as diffusers and concentrators. HAWT is more popular because they have better efficiency, but only suitable for places with high wind speed. In contrast, VAWT works well in places with relatively lower strength, but constant wind (Reigler 2003). The blades are not needed to orient in wind direction as it can work always in the same direction though wind comes from any direction. (Ragheb 2012)

Due to better aerodynamic behavior and more efficient in the large scale, HAWT was the popular choice of the researchers. But several factors are turning the head of researchers towards the field of VAWT. They are, VAWT may be more appropriate than HAWT in small scale. VAWTs are suitable for electricity generation in the conditions where traditional

HAWTs are unable to give reasonable efficiencies such as low wind velocities and turbulent wind flows. VAWT can operate without any dependence on wind direction. The quiet behavior is more attractive for highly populated places. The cost of complex structure of HAWT blades is higher than simpler VAWT blades. Because of the stalling behavior it can withstand gust wind, which makes it much safer during those weather conditions. This type of rotor can be installed in remote places, away from the main distribution lines and places where large wind farms cannot be installed due to environmental concerns. Some place needs small scale dispersed generation units where VAWT is suitable. (Bishop and GAJ 2008)

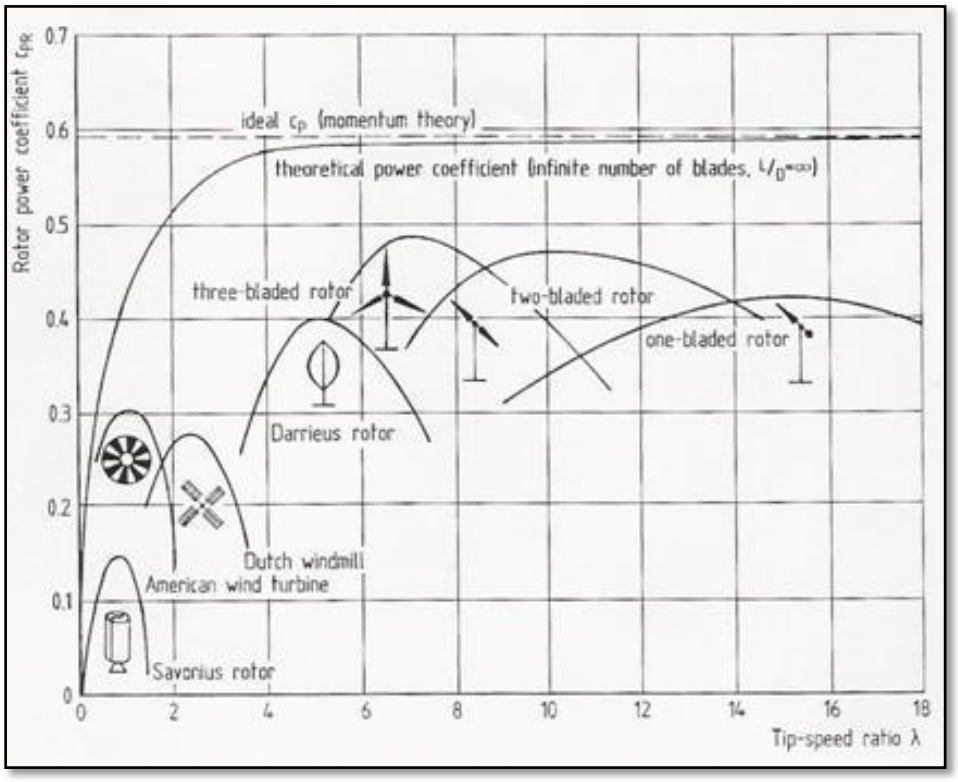

FIGURE 1-2: Power Coefficient (C_p) vs. Tip Speed Ratio (λ) For Various Wind Turbines (HAU 2006)

1.4 Vertical Axis Wind Turbines

In general, VAWT is driven by two types of forces of wind, drag and lift force. Savonius rotor is the simplest kind of VAWTs is a drag-type configuration and a bit complex type is Darrieus rotor which is lift-type configuration.

Savonius Rotor: The operation of Savonius rotor depends on the difference of drag force when the wind strikes the concave and convex part of the semi-spherical blades. The flow energy utilization of Savonius rotor is lower than that of Darrieus rotor. Hence this type of turbine is generally not used for high-power applications and usually used for wind velocimetry applications (Islam, Ting and Fartaj 2008). The greatest advantage of a Savonius rotor is its ability to self-start in contrast to other 'Lift type' VAWTs (Mohamed, et al. 2011). Recently, some generators with high torque at low rotational speed, suitable for small-scale wind turbines, have been developed, suggesting that Savonius rotors may yet be used to generate electric power (T. Hayashi, et al. 2004).

Darrieus Rotor: The energy is taken from the wind by a component of the lift force working in the direction of rotation. Lift force is perpendicular to the resultant of two velocity component of wind velocity and relative velocity of airfoil to the shaft. These types of turbines have highest values of efficiency among VAWTs and the tip speed ratio can be much higher resulting in a much higher rpm. But generally suffer from problems of low starting torque and poor building integration.

Combined Savonius and Darrieus Rotor: Since the Darrieus rotor is not self-starting; a blended design with Savonius blade can make the hybrid which can make it starting and more efficient than any of the single rotor.

1.5 Wind Energy Utilization

Wind is the generating electricity currently less than 3.5% of US and barely 4.5% of world electricity consumption. Though the popularity of wind as energy source is increasing rapidly but it will still generate a few portions of US and world electricity requirements by 2030. The scarcity of resources, increasing demand of energy and concern of global climate change is pushing hard to increase the efforts to find viable energy alternatives. Some of the renewable energies may not be achievable or sustainable, some are local and limited. Other than fossil fuel the only hope is solar and wind. To be the significantly larger contributor to generate global electricity, the wind power needed to be more efficient.

According to the World and European Wind Energy Associations, installed global wind capacity reached 197, Giga-watts by the end of 2010, with just over 3,000 MW of that total located offshore. World wind power generation capacity in 2013 was estimated at 318 GW, which is 13% higher than previous year (REN21 2014)

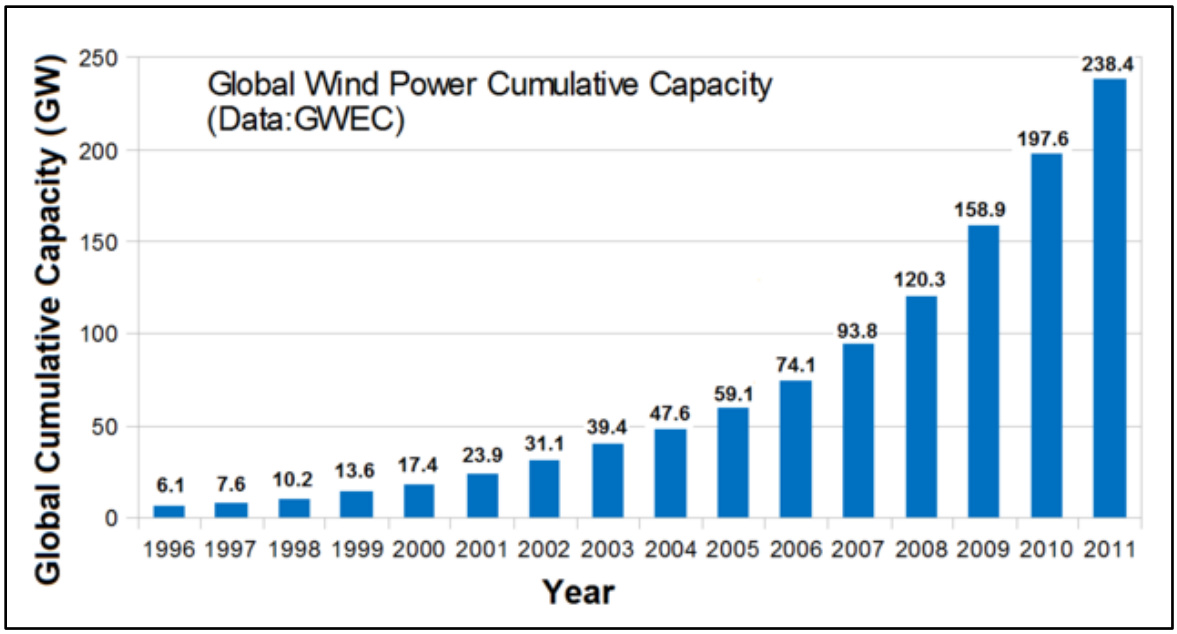

FIGURE 1-3: Global Cumulative Capacity of Wind Energy (GWEC 2012)

Renewable energy sources provided about 12% of total U.S. utility-scale electricity generation in 2013. The largest share of the renewable-generated electricity came from hydroelectric power (30%), followed by biomass (25%) and wind (19%) (Administration 2013). According to U.S. energy reports, US wind power generation capacity in 2005 was 17 GW; it had grown to 167 GW by 2013.

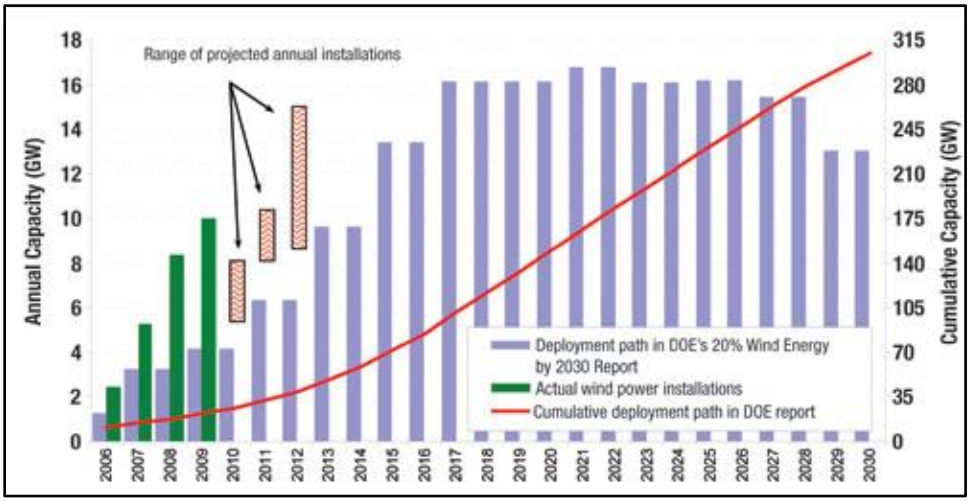

FIGURE 1-4: Projected and Actual Installation of Wind Energy by DOE (ADMINISTRATION 2013)

China has the highest capacity in wind energy generation, followed by the United States, Germany and Spain (REN21 2014).

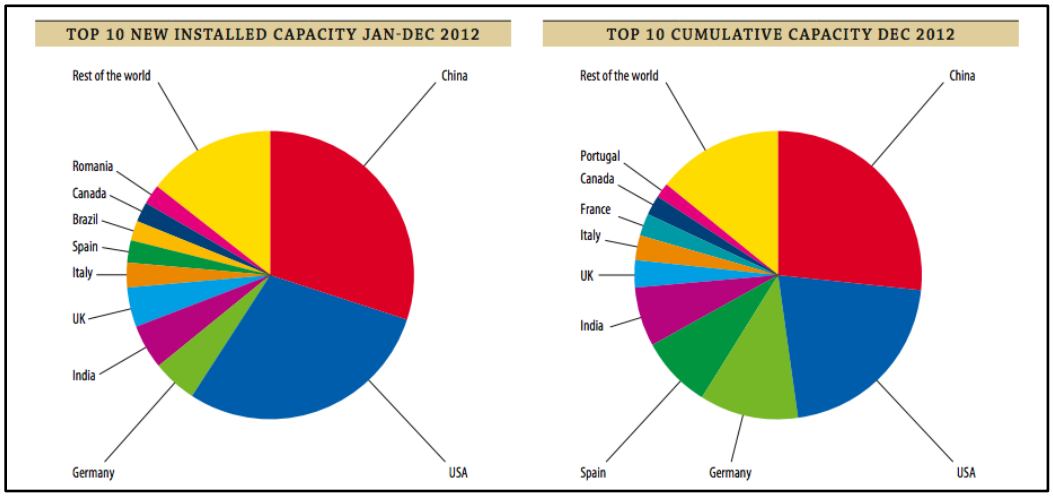

FIGURE 1-5: Wind Energy Generation Capacity by Country (TECHNICA 2012)

1.6 Motivation of Research

On efficiency measurement, HAWT is the popular to the researchers. But it works best in places where the wind is not disturbed and has high wind velocity. But the inherent advantages of facing the wind direction, simplistic design, cheap technology for construction, lower wind start-up speeds, easier maintenance, and are relatively quiet are turning the focus to VAWT. Specially in areas where wind power is low and do not always have a high wind velocity. The designs of VAWTs are simple and operation is based on the difference of the drag force on its blades.

The previous researcher from this lab also experimented on three bladed Savonius wind turbine and concluded that change of blade shape can have real impact on this kind of turbine. The turbine model without any overlap at higher Reynolds number shows better aerodynamic co-efficient. (Morshed, et al. 2013). The outcome provided the basic motivation to design newer blades which may help to improve the performance of VAWT.

1.7 Scope of Research

Currently many researchers have been investigating the characteristics to improve the efficiency of different VAWTs and to find out a design which can provide maximum output. Numerical and Experimental research is going on to find the optimum number, shape of blades, overlap ratio and number of layers for Savonius rotor. On the other hand investigation is going on aerodynamic behavior of the blades of VAWT to increase the value of starting torque.

Comprehensive dynamic study using both experimental and numerical methods has not been extensively studied on airfoil as VAWT blade, if studied at all. In this current research the

shape of airfoil blades have been changed to investigate experimentally and numerically at various tip speed ration. Dynamic torque measurement method has been performed for experimental investigation. Commercially available software ANSYS FLUENT have been used for the numerical analysis.

1.8 Objectives of the Research

The objective of this research is to find the highly efficient VAWT by studying the aerodynamic characteristics of the blades of Savonius rotor. In order to investigate the improvement of the performance the following steps were set for the research:

1. To design the models using 3-Dimentional CAD software Solidworks and ANSYS;
2. To generate numerical mesh around all the turbine models using FLUENT;
3. To create a Fluid flow field around the models using k-ε turbulence model of FLUENT for study; then to determine the drag coefficient, lift coefficient, pressure contours, velocity contours and torque coefficient at various wind speed;
4. To calculate the numerical power coefficient using torque coefficient;
5. To design and fabricate Savonius rotor wind turbine scale models with optimum blade numbers and selected shapes;
6. To measure torque in front of subsonic wind turbine for all models at different wind speed with the help of dynamic torque sensor. Then calculate torque and power coefficient from experimental values

   And
7. To compare the numerical and experimental results.

1.9 Outline of the Thesis

The thesis is presented in the following direction.

- A brief description of the findings of both experimental and numerical investigation for different models of VAWT from previous research outcomes.
- The method of this research; outlines of experimental setup, design development of turbine models, governing equations, experimental and numerical methodology.
- Discuss the result yielded from the experiment.
- Final conclusion on the current study, recommendation and guidance based on the laggings for the future investigation.

CHAPTER 2

2 Literature Review

2.1 Introduction

Researchers have been conducting lots of experiments on HAWT, because of its high efficiency. In some way, researchers have been trying their best to find the best from Darrieus rotor. Meanwhile, significant numbers of researchers have been working to improve the aerodynamic characteristics of Savonius turbine. These researches are numerical and theoretical prediction for flow around the wind turbines and from that it varies from research laboratories to full scale simulation. The extensive amount of work has been carried to find a sustainable solution of wind energy. Around the globe researchers have been experimenting on HAWT and Darrieus rotor for large scale energy production and Savonius rotor for small scale usage. Based on the conclusion of those experiments, hybrid turbines are also a focus of the researchers. A brief discussion of Numerical analysis and experimental work on VAWT will be discussed in this chapter.

2.2 History of Wind Turbine

2.2.1 The Wind Turbine

Windmills were used in Persia (present-day Iran) as early as 200 B.C. Pumping water had been the role of wind turbine for many centuries. The Netherlands used wind mills for dewatering large areas from the 13th century onwards. The ending of the nineteenth century divided the two development periods; the earlier is known as ancient development period and

later as the modern development period. In July 1887, Scottish academic James Blyth installed the first electricity-generating multi bladed HAWT to charge his battery for holiday light in Scotland. (Price 2009).

By 1900, there were about 2500 windmills almost produced 30 MW of electricity for mechanical loads such as pumps and mills in Denmark. By 1908 there were 72 wind-driven electric generators from 5 kW to 25 kW and by 1930 wind farms for electricity were common in USA.

2.2.2 Vertical Axis Wind Turbine

From history book, it was found that about 1300 A.D a Syrian cosmographer Al-Dimashqi drew a vertical axis windmill (Shepherd 1990). It was a two storied wall structure with milestones at the top and a rotor at the bottom. It had latter with spooked reel with 6 to 12 upright ribs that covered with cloth. It was found that this type of windmill had been in operation in 1963 which used to produce an estimated 75 hp (at efficiency of 50% at wind speed 30 m/s). Each windmill milled one ton of grain per day (Wulff 1966).

2.2.3 Savonius and Darrieus Type Wind Turbine

The Savonius wind turbine was first used by a Finnish Engineer S. J. Savonius in 1931 (Savonius 1931). The design of his rotor was S-shaped with two semi-circular buckets with small overlap. At that time this rotor was successfully used as an ocean current meter.

In 1931, G. J. M. Darrieus in France patented another VAWT named Darrieus vertical axis rotor. This type of rotor was not self-starting.

2.3 Review on Savonius Rotor

The optimum output from the wind energy is the key objective of the investigation and different aerodynamic shapes of the blades are designed to verify the outcome. Numerous investigations had been carried out in the past to study the performance characteristics of Savonius rotor. These investigations included wind tunnel tests, field experiments and numerical studies. Blade configurations were studied in wind tunnels to evaluate the effect of aspect ratio, number of blades, overlap and gap between blades, effect of adding end extensions, end plates and shielding.

2.3.1 Changing the Overlap Ratio of Blade

The performance of two bladed Savonius turbine with five overlaps of 16.2%, 20%, 25%, 30% & 35% were investigated. Among them 16.2% overlap condition showed maximum power extraction. The pressure drop across the rotor from upstream to downstream as well as, maximum pressure difference across the returning bucket was displayed in the same condition which eventually indicated the better overall aerodynamic torque and power. (Gupta, Das, et al. 2012)

Three bladed Savonius rotor with different overlap ratio was taken care for another experiment. Ratio of 0.0, 0.12 and 0.26 had been used for different Reynolds number (Re). The model with no overlap ratio showed better torque coefficient for lower Re, better power coefficient at higher Re and with the increase of tip speed ratio. (K. N. Morshed 2010)

(Biswas et al. 2007) conducted the experiment on three bladed Savonius turbine in front of sub-sonic wind tunnel with no overlap and for overlap conditions in the range of 16% to 35%. They found out that, at no overlap condition, maximum power factor is 36% without blockage correction at TSR of 0.50, and 28% with blockage correction at TSR of 0.46. With

the increase of overlap ratio, the values of power-coefficient decreased for blockage effects. Power coefficients increased with the increase of overlap ratio up to a certain limit and afterwards start decreasing even the overlap is increased. From this experiment, the maximum power coefficient was found 47% without blockage correction and 38% with blockage correction at 20% overlap.

2.3.2 Changing the Shape of Blade

(Qasim et al. 2011) worked with impeller scoop-frame type with movable vanes wind turbine VAWT. The objective was to maximize the drag factor by closing the vanes on convex shape and open when air hit the concave part. Due to movement of vanes for and against of wind, a higher drag factor had worked on the impeller scoop-frame type with movable vanes, and had higher efficiency than flat vanes.

(Manzoor et al. 2008) experimented on Savonius rotor to compare the performance of twisted blade. Initially they carried the experiment with two vertical, semi-circular curved blades and then with twisted blade with the angle ranging from 0° to 60°. From the analysis of wind flow over various configurations of the rotor blades they have concluded that, the maximum efficiency of 33.85% had been found at θ=45° compared to 25.6% without twist. This twist increases the positive wetted part in the side projected area which results an increase in the average projected area. At the same twist angle, both the RPM and torque were also obtained higher than without twist.

(Saha et al. 2006) studied the performance of twisted blade. All the tests were carried out in a three-bladed system with a blade aspect ratio of 1.83. The study showed that, a potential of smooth running, higher efficiency and self-starting capability had been there for twisted blades compared to semicircular blades. Comparatively larger twist angle provides maximum

power and better starting characteristics at lower wind velocity. The optimum performance is displayed at low airspeeds of 6.5 m/s and twist angle of α =15° in terms of starting acceleration and maximum no load speed.

(Ghatage and Joshi 2012) have done further experiment by changing twist of blade as well as the number of blade. They have studied with both regular blade and twisted blade. The experiment concluded that two blades with twist enhance the efficiency of turbine. In their experiment the two-bladed 30° twisted bladed turbine gave the better power coefficient. It was concluded that the twisted blade attributes relatively higher drag on the turbine surface.

2.3.3 Changing the Stage

(Ghosh, et al. 2009) have experimented Single- and three-stage modified Savonius rotors, which are extensively tested in front of an open jet wind tunnel. With the increase in the Reynolds number both the single- and three-stage rotors shows higher coefficient of power. The three-stage rotor showed positive and uniform coefficient of static torque. Here the number of blade also had some effect. The coefficient of static torque differed with the change of blade number in a three-stage rotor.

(Hayashi et al.2005) experimented a wind tunnel test to improve the starting characteristics of Savonius rotor with and without guided vanes. They have concluded that, the three staged rotor had better torque coefficient than single stage rotor. The guide vanes further increased the torque coefficient.

(Kumbernuss, et al. 2012) studied two-staged Savonius-type turbines with different number of blades, the shape of the blades, the overlap ratio and the phase shift angle. The wind turbines were tested under four different wind speeds of 4m/s, 6m/s, 8m/s and 10m/s. There were three turbines with the overlap ratios of 0, 0.16 and 0.32. Before testing those in an

open wind tunnel, the wind turbines were adjusted to the phase shift angles (PSA) of 0, 15, 30, 45 and 60 degrees under different air velocities. The overlap ratio of 0.16 produced the better performance among the three, followed by the 0.32 overlap ratio. At lower air velocities the larger phase shift angles and at higher air velocities smaller phase shift angles will produce better performance of the turbines.

(Saha et al. 2008) conducted a wind tunnel test to assess the aerodynamic performance of Savonius rotor systems with different stages. Both semicircular and twisted blades had been used in each case. Experiments were carried out to optimize the different parameters like number of stages, number of blades (two and three) and geometry of the blade (semicircular and twisted). It was concluded from this experiment that, two-stage rotor showed a better performance characteristics when compared the three-stage rotor. As the number of stages was increased, the inertia of the rotor was found to increase thereby reducing its performance. This was independent on the blade geometry. Two-bladed system gave optimum performance and in a two bladed system, the performance of twisted-bladed rotor was superior to the semicircular-bladed rotor.

2.3.4 Aerodynamic Characteristics

(Diaz et al. 1991) analyzed to find the drag and lift coefficients of a Savonius wind turbine to find the aerodynamic performance. They found that at a tip-speed ratio of $\lambda = 1$ the rotor operated with maximum efficiency, in terms of power coefficient. For either increase or decrease of tip-speed ratio the drag coefficient decreases sharply. They also suggested that, around tip-speed ratio $\lambda = 1$, Savonius rotor operates most efficiently, where there is almost no effect of change of lift force due to the coefficient remains constant at 0.5.

(M. Rahman, K. N. Morshed, et al. 2009) (2010) experimented on the Drag and Torque characteristics of three bladed Savonius Wind Turbine. The turbines with no overlap has better drag and torque characteristics. They also performed Aerodynamic performance analysis on three bladed Savonius wind turbine and concluded that higher reynold number showed better aeorodynamic behavoir for no overlaping blades.

(Carrigan, et al. 2012) had the objective to introduce and demonstrate a fully automated process for optimizing the air foil cross-section of a VAWT. The objective was to maximize the torque while enforcing typical wind turbine design constraints such as tip speed ratio, solidity, and blade profile. This work successfully demonstrated a fully automated process for optimizing the air foil cross-section of a VAWT. As this experiment was not an extensive study, so they had suggested further research and development.

2.4 Review on Darrieus Rotor

Like Savonius, many experiments have been studied to find the optimum performance of Darrieus rotor. These investigations included mostly numerical studies and some are simulated in wind tunnel as well as in field. Aerodynamic characteristics were studied to evaluate the effect of blade shape and angle, material and configurations. Some researchers tried to change the external factors to improve the starting characteristics of Darrieus rotor.

2.4.1 General Findings

(Howell, et al. 2010) experimented on small scale Darrieus rotor. A combined experimental study in wind tunnel and computational study was done to find the aerodynamics and performance. In this experiment they changed wind velocity, tip-speed ratio, solidity and rotor blade surface finish. It was found that, below a critical wind speed (Reynolds number of

30,000) a smooth rotor surface finish degraded the performance of the turbine. The tests also showed that both two and three bladed rotor models had produced highest performance coefficient, but the three bladed models did so at a much reduced Tip Speed Ratio. Considering errors and uncertainties in both the CFD simulations and the wind tunnel measurements, computational study displayed reasonably good agreement with the experimental measurements. Stronger tip vortices were created at phases with higher amounts of lift present.

(Beri and Yao 2011) studied to show the effect of camber airfoil for a self-starting Darrieus turbine. For this purpose they have used three bladed NACA 2415 camber airfoil and simulated in different tip speed ratio. The experiment results showed that, camber airfoil have the characteristics of self-starter. Though for same power coefficient the efficiency was less than the non-self-starting airfoils.

2.4.2 Changing the Shape of Blade

(Hameed and Afaq 2012) designed a straight symmetrical blade for a small scale Darrieus rotor using beam theories. They changed the design parameters of the blade like solidity, aspect ratio, pressure coefficient etc. for experiment purpose. Then the blade design was analyzed at extreme wind conditions where maximum values of deflection and bending stresses were determined at peak values of aerodynamic and centrifugal forces. It was concluded that keeping the maximum stresses and deflection within acceptable range, the wall thickness of the blade could be optimized by reducing weight of the blade.

(Armstrong et al. 2012) investigated the aerodynamics of a high solidity Darrieus rotor through wind tunnel tests limited at Re >500,000 for full size operating turbine. Straight blades and canted blade showed different flow separation behavior. Canted blades

experiencing less flow reversal on their upwind pass and recovering attached flow before $\theta = 180^0$. Much less flow separation was noted relative to the straight blades at the same blade speed ratios even for the peak blade ratio $\lambda = 2.1$. Canted blades increased the power and reduced the blade speed ratio at which peak power occurred. The addition of fences, which acted to impede span wise flow on the swept blades, reduced the blade speed ratio at peak power to about $\lambda = 1.9$, presumably with a flow that is more similar to the straight blade case.

2.4.3 Different Other Numerical Investigations

(Castelli, et al. 2013) presented a model for the evaluation of aerodynamic and inertial contributions to a VAWT blade deformation. Solid modeling software, capable of generating the desired blade geometry depending on the design geometric parameters, is linked to a finite volume Computational Fluid Dynamic (CFD) code for the calculation of rotor performance and to a Finite Element Method (FEM) code for the structural design analysis of rotor blades. Flow field characteristics were investigated for a constant unperturbed free-stream wind velocity of 9 m/s, determining the torque coefficient generated from the three blades. The computed inertial contribution to blade deformation resulted quite higher with respect to the aerodynamic one for all the analyzed blade shell thicknesses. Both inertial and aerodynamic displacements resulted higher at blade trailing edge than at leading edge. They suggested for further investigation on the influence of this blade section deformation on the aerodynamic performance.

(Carrigan, et al. 2012) had the objective to introduce and demonstrate a fully automated process for optimizing the airfoil cross-section of a VAWT. The objective was to maximize the torque while enforcing typical wind turbine design constraints such as tip speed ratio, solidity, and blade profile. This work successfully demonstrated a fully automated process

for optimizing the airfoil cross-section of a VAWT. As this experiment was not an extensive study, so they had suggested further research and development.

2.5 Review on Hybrid Rotor

(Wakui, et al. 2005) experimented to find a suitable hybrid configuration of Darrieus lift type and Savonius drag-type rotors for stand-alone wind turbine-generator systems. They experimented with Savonius rotor inside the Darrieus rotor and Savonius rotor outside the Darrieus rotor. The maximum power coefficient points showed that Savonius rotor inside the Darrieus rotor had fine operating behavior to wind speed changes and could be compactly designed because of a shorter rotational axis. This is an effective way for stand-alone small-scale systems. The results of evaluating the net power extraction under field wind conditions confirmed that Savonius rotor outside had been more effective in a small-scale system. However, under wind conditions involving short blowing duration, Savonius rotor inside had been more effective due to the drop in the effective electric power coefficient. Also the Savonius rotor outside had some starting problem.

(Gupta et al. 2008) has compared one simple Savonius and the other combined Savonius–Darrieus wind rotors. The Savonius rotor was a three-bucket system having provisions for overlap variations. The Savonius–Darrieus rotor was a combination of three-bucket Savonius and three-bladed Darrieus rotors with the Savonius placed on top of the Darrieus rotor. This comparative study showed that, there had been a definite improvement in the power coefficient for the combined Savonius–Darrieus rotor without overlap condition. Combined rotor without overlap condition provided an efficiency of 0.51, which was higher than the efficiency of the Savonius rotor at any overlap positions under the same test conditions.

CHAPTER 3

3 Methodology

The research objective is to find the highly efficient Vertical Axis Wind Turbine by studying the aerodynamic characteristics of the blades of Savonius rotor. The basic parts are divided into three parts.

The foremost part of this research is numerical investigation. This computational investigation was done using academically available ANSYS. The flow field was designed on a 2-D model. The mesh was generated with ANSYS and basic investigation was run on FLUENT to determine the aerodynamic coefficients; such as drag, lift, and torque coefficient. And values of forces, velocity and torque are extracted and then used to calculate torque and power coefficient.

The next step is to create few prototype blades of models and some tests were conducted in front of a subsonic wind tunnel varying the wind speed. Torque, wind speed and rotational speed are measured and used to calculate torque and power coefficient.

Final step is to study both numerical and experimental results and to make a final conclusion.

This chapter also describes the basic experimental setup which is applied for both numerical and experimental study; in detail method of the numerical model selection, validation and numerical technique to solve fluid flow, experimental set up, fabrication of rotor blade and experimental data measurement procedure.

3.1 Experimental Design

A subsonic wind tunnel with the capacity to change the wind speed is considered to produce wind velocity. The experiment needs to be done under different wind velocity and different blade shapes are created to compare different results.

The NACA 4-digit series is chosen to create air foil. Because this type of airfoil has some good aerodynamic characteristics which match the characteristics of Savonius type VAWT. Those are good stall characteristics and little roughness affect, relatively high drag, low lift coefficient. The analytical equations describe the camber (curvature) of the mean-line (geometric centerline) of the airfoil section and also the distribution of section thickness along the length of the airfoil; are used to generate this kind of airfoil.

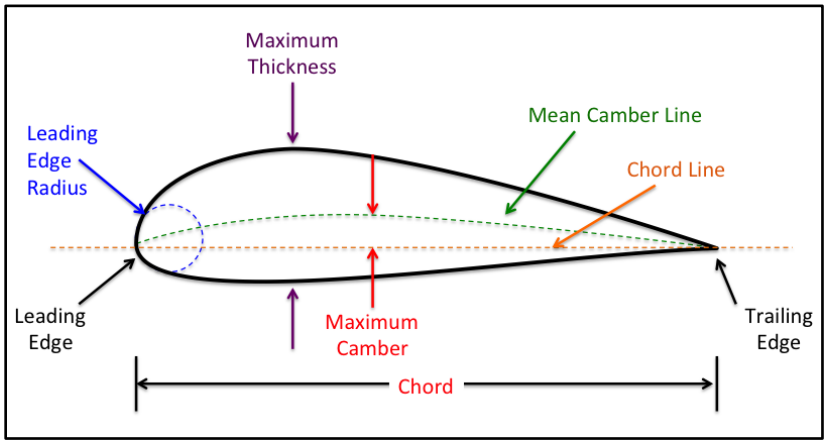

FIGURE 3-1: Airfoil Terminology

Based on previous experimental results, it is optimized that three blades provide best result. The blades are placed 120^0 apart for the rotor model. The whole turbine model assembly is installed in a frame. The same experimental setup is also portrayed in computational simulation.

The air is the only fluid for the experiment. The models are tested using the interchangeable design varying wind speed of 10 m/s, 11.5 m/s, 12.5 m/s and computationally at15 m/s. This

wind speeds produce different angular speed of the rotor and the torque. Based on same base load, the torque is measured and angular speed is measured with the device. The effect of temperature can be ignored in this measurement technique as the experiment is carried out at atmospheric temperature. For the regular room temperature the air density $\rho = 1.2\,\frac{kg}{m^3}$ and air viscosity $\mu = 1.983\,\frac{kg}{ms} \cdot 10^{-5}$

3.2 Mathematical Relations

The power is nothing but the rate of change of angular momentum of wind stream just at inlet of the test section. Power produced by the rotor was measured from torque and the angular speed using equation (3.5). The tip speed ratios (λ) were calculated using the measured angular speed values in equation (3.4). The torque coefficients (C_q) can be calculated using the measured dynamic torque data using equation (3.6) for all the models. Power coefficient can be calculated using the measured torque and angular velocity of the rotor in equation (3.7).

Rotor Area $$A = D.H \quad [3.1]$$

Angular Velocity $$\omega = \frac{2\pi N}{60} \quad [3.2]$$

Reynolds Number $$Re = \frac{VD}{\nu} \quad [3.3]$$

Tip Speed Ratio $$\lambda = \frac{\omega D}{2V} \quad [3.4]$$

Power $$P = T\omega \quad [3.5]$$

Torque Coefficient $$C_q = \frac{T}{0.5\rho A V^2 R} \quad [3.6]$$

Power Coefficient

$$C_P = \frac{P}{0.5\rho A V^3} \quad [3.7]$$

Drag Coefficient

$$C_d = \frac{F_d}{0.5\rho A V^2} \quad [3.8]$$

Lift Coefficient

$$C_l = \frac{F_l}{0.5\rho A V^2} \quad [3.9]$$

The schematic diagram of the Savonius rotor cross-section with the components of drag forces on each blade is shown in Figure 3-2.

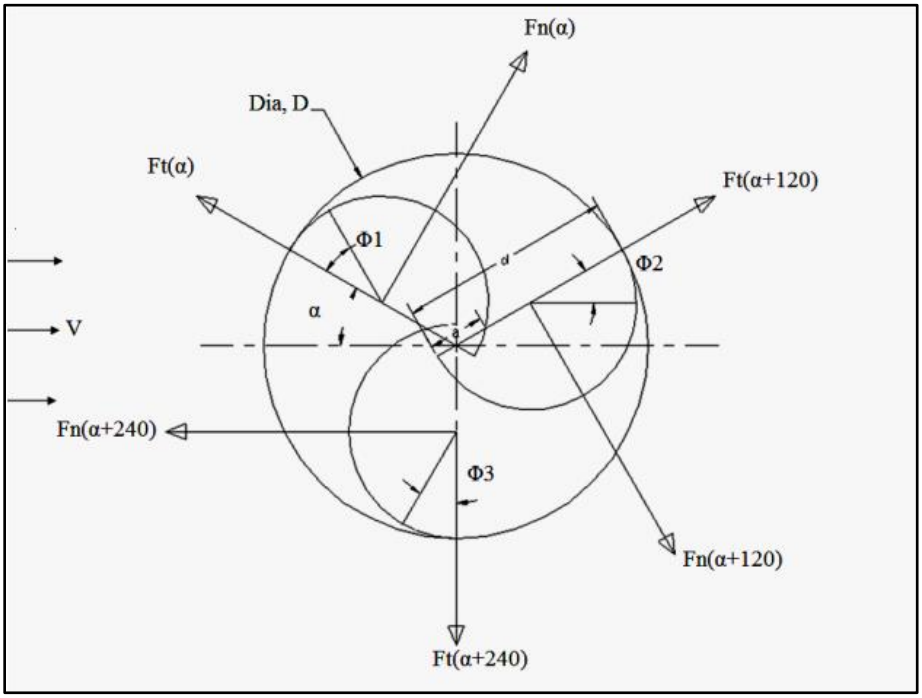

FIGURE 3-2: Schematic Diagram of the Drag Force Components on Model Cross-Section

Savonius wind turbine is drag type VAWT where the lift forces are considered to be negligible. When the wind strikes the blade surfaces of the model, two components of drag force are generated on each blade surface. Normal drag force (F_N) acts perpendicular on the blade surface and tangential drag force (F_T) acts along tangential direction on each blade.

3.3 Numerical Method

The first step is the optimization process is generating the geometry. Different blades of VAWT have been created using Solidworks and ANSYS. This geometry is described as a set of Cartesian coordinates and is passed to the mesh generation module. For the purpose of numerical analysis, Computational Fluid Dynamics (CFD) code FLUENT 2-D is used and five different models are numerically examined at the different wind speed and compared among them.

3.3.1 Blade Profiles

Five different models were created for this numerical analysis. With overall diameter of 8.5 inch, the shaft diameter at the center is 0.5 inch. Five different blade profiles: semi-circular, quarter-circular, and three airfoils NACA5510, NACA7510 and NACA9510 had been created. The basic semi and quarter circular shapes experimented in many researches, which will help to compare the basic shapes with airfoil shape.

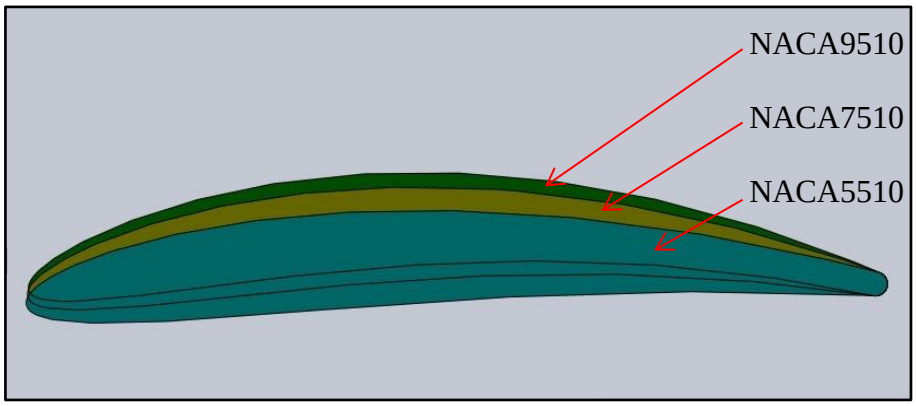

FIGURE 3-3: Comparative View of NACA 5510, NACA7510 and NACA9510

NACA 4-digit airfoil series is popular way to create airfoil. The first digit specifies the maximum camber in percentage of the chord. The second indicates the position of the maximum camber in tenth of the chord. The last two digits provide maximum thickness in

percentage of the chord. (Airfoil Tools n.d.) For our research work we considered to change the maximum camber and keeping the position of that camber and thickness constant

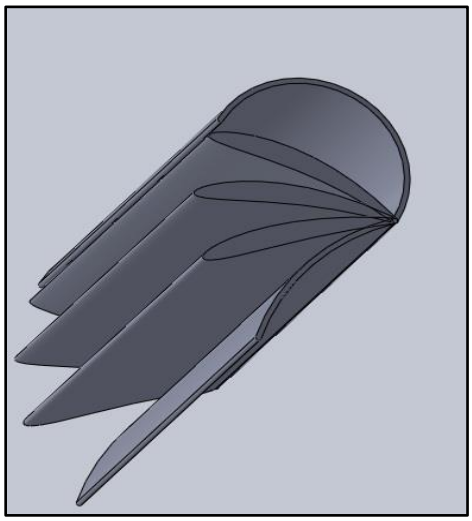

FIGURE 3-4: Isometric View of All Five Blade Profiles

Then all the profiles had taken into academically available 3-Dimensional CAD software Solidworks to create solid model. Then ANSYS Design Modeler were used to make the 2-D profiles and generating mesh.

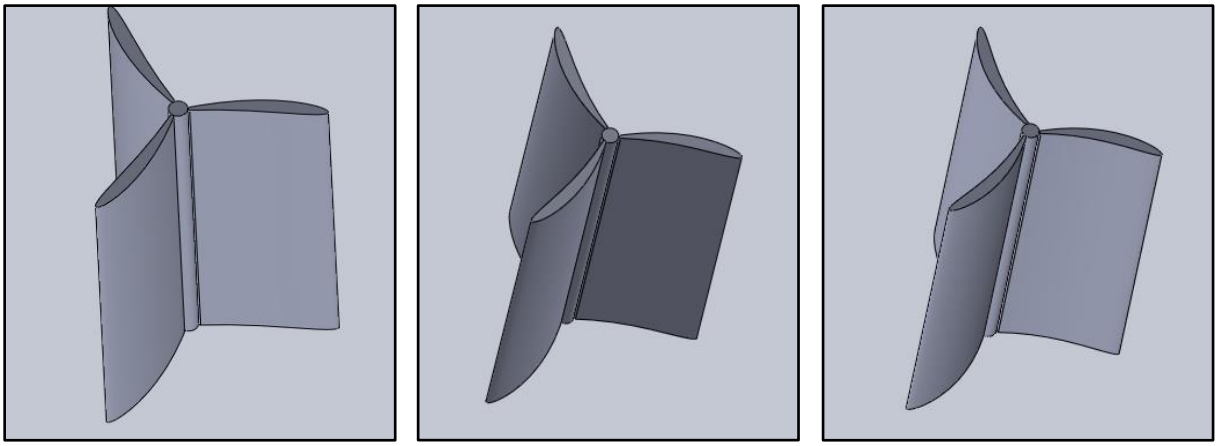

FIGURE 3-5: Isometric View of Rotor Models of NACA5510, NACA7510 and NACA9510

3.3.2 Mesh

For 2-Dimensional analysis a mesh was generated around the rotor using ANSYS Mesh. The exit of wind tunnel is thought to be the inlet in the grid here. Then in the environment the rotor is placed. The environment and the rotor are separated by interface. This interface is also required for sliding mesh technique. A total created number of nodes are 5476 for NACA5510, 6077 for NACA7510 and 6137 for NACA9510. For quarter circular shape 6675 and semi-circular shape 6437 Nodes were created.

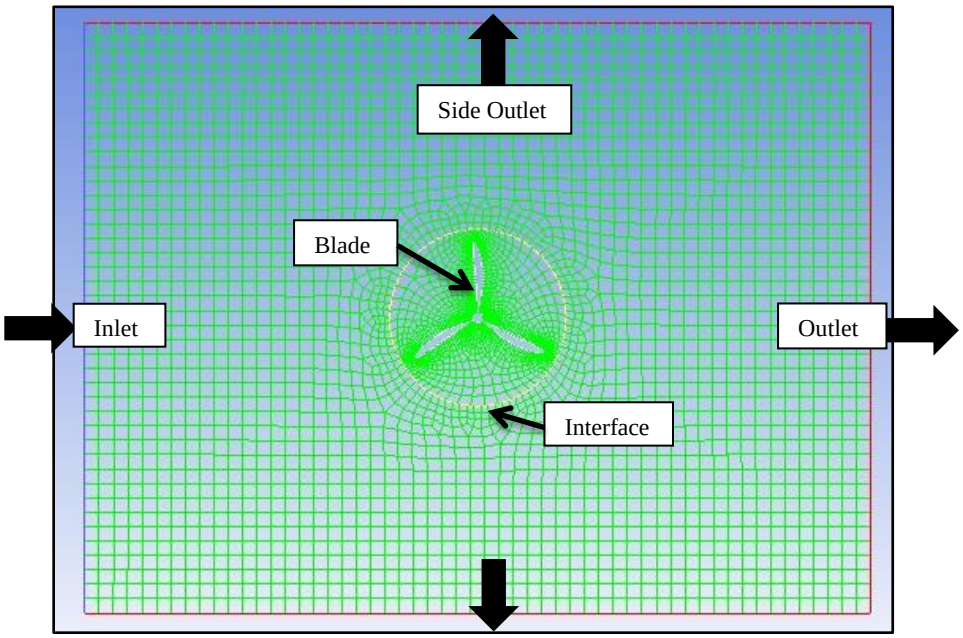

FIGURE 3-6: Mesh around the Airfoil Using ANSYS

The models were simple extrusion, so a 2-D simulation had been done here because it would provide the same result of 3-D model. CFD ANSYS solver was used to create the mesh. The orthogonal grid was very refined around the rotor blade and the interface which means inlet of air towards rotor area and with a smooth transition at downstream and radially. The Air-inlet, outlet and side outlet (top and bottom) are shown in the figure 3-6. All the meshes were generated with three blades. The computational domain was measured 40in X 30in.

3.3.3 Numerical Model:

A systematic, iterative numerical study on various blade shapes was performed using the commercial software package ANSYS/FLUENT (version 14.0) from ANSYS Inc. To simulate air flow around the rotor, pressure based solver and transient solution were used and to rotate the rotor sliding mesh technique is used. The k-ε turbulence model was used for the flow simulation. The standard k-ε turbulence model (Launder and Spalding 1972) is a semi-empirical model. This model is based on the transport equations for the turbulence kinetic energy (k) and its dissipation rate (ε). The model transport equation for (k) was derived from the exact equation. On the other hand physical reasoning and little resemblance to its mathematically exact counterpart helps to obtain the model transport equation for (ε).

3.3.4 Numerical Procedure

Boundary conditions were changed to vary different procedure. The left side of the grid was assigned as inlet where it was considered that air is flowing in single direction. The air hits the rotor blade and helps rotating and then going away. This right side was main outlet and top and bottom were side outlets at atmospheric pressure. The air velocity at the inlet was considered as 10 m/s, 11m/s, 12.5m/s and 15m/s. Blades were considered as moving wall. For uniformity of the results all the models were kept at the same starting position.

The environment where the air was flowed around the rotor was assumed turbulent. As the outlet is directly against the open door and side outlet is against the wall at a distance so the backflow turbulence was considered higher for regular outlet. The momentum, turbulent kinetic energy and dissipation rate were calculated using Second Order Upwind method.

Numerical simulation provides the pressure and velocity values at all nodal points of flow domain around the rotating blades. Solidity is another important parameter dictating the

rotational velocity at which the turbine reaches its maximal performance. For all the models continuity, X and Y velocity, Kinetic energy (k) and dissipation rate (ε) had the same convergence criteria.

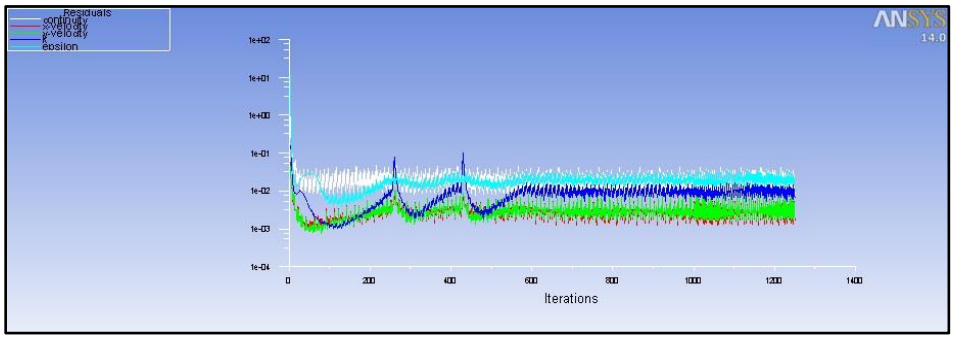

FIGURE 3-7: Residual Convergence of Model NACA5510 at 12.5 m/s

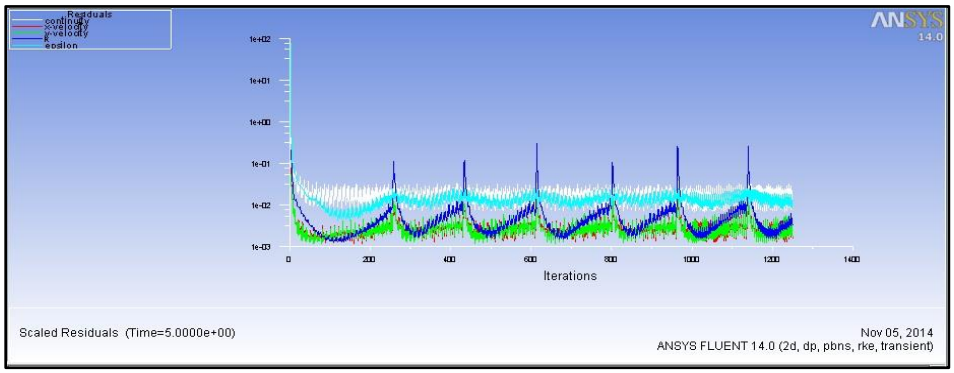

FIGURE 3-8: Residual Convergence of Model NACA7510 at 10 m/s

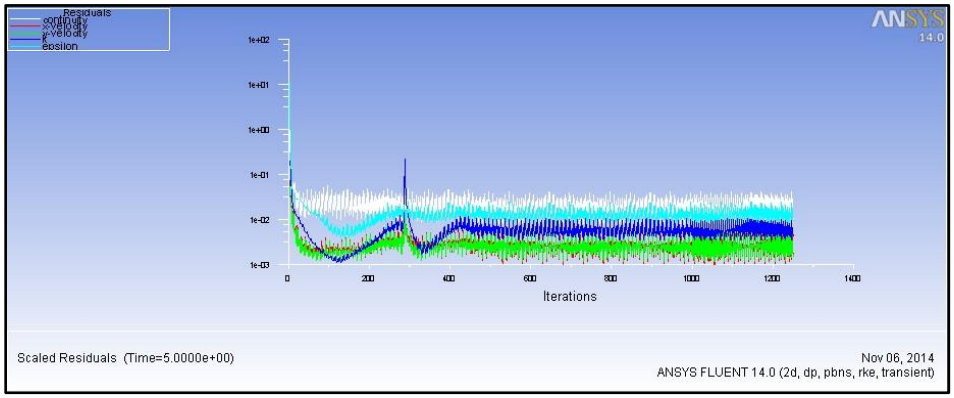

FIGURE 3-9: Residual Convergence of Model NACA9510 at 15 m/s

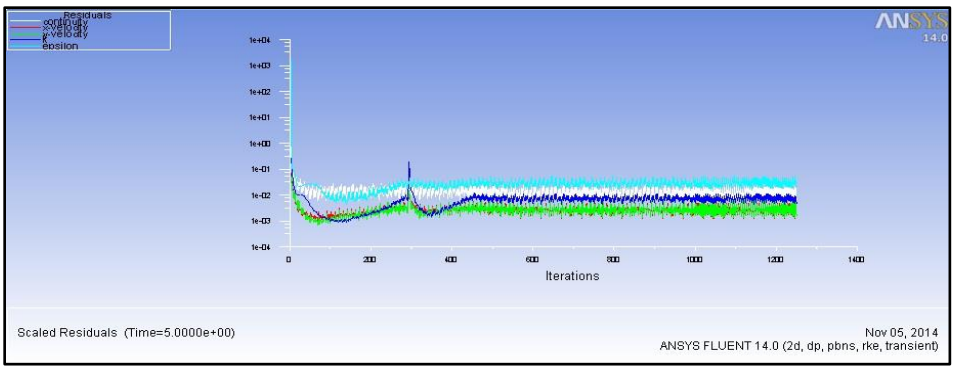

FIGURE 3-10: Residual Convergence of Quarter Circular Bladed Model at 10 m/s

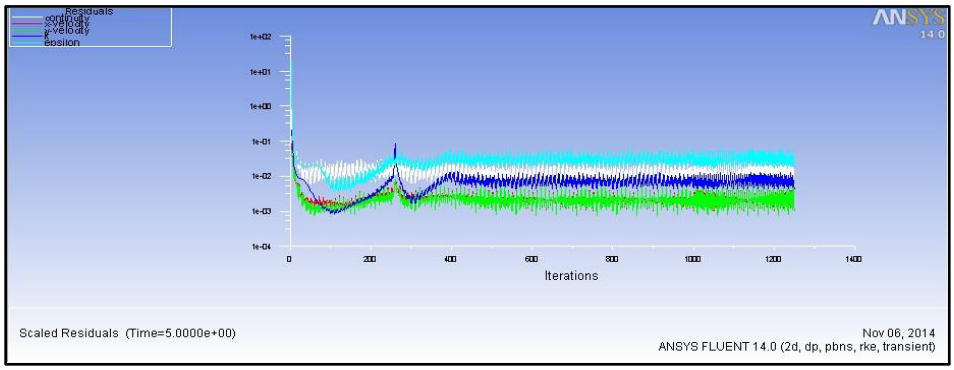

FIGURE 3-11: Residual Convergence of Semi Circular Bladed Model at 15 m/s

For transient solution, after few time-steps the residuals shows same pattern. After few seconds all the models showed a pattern for the convergence. Figure 3-7 to 3-11 show residuals of different models at different speed.

As a rotating device, all the characteristics residual display a sinusoidal curve. But the main characteristic on which the steadiness depends for all the models is Kinetic energy (k). From the above figure it is displayed that the residual of kinetic energy changed suddenly from low to high and low and then remains steady for the steady wind flow. Velocity provides the main role behind the kinetic energy. Continuity and Epsilon has little change over the time.

It has seen that, NACA profile bladed rotors are unsteady for lower wind speed for almost 5seconds. With increment of wind speed the pattern developed after 2-3 seconds. On the other hand, circular shaped bladed rotor developed steady pattern soon for any wind speed.

3.4 Experimental Method

Similar to computation analysis blades were manufactured and those rotors were tested in front of the wind tunnel varying wind speed.

3.4.1 Subsonic Wind Tunnel

The subsonic wind tunnel is already available which is 12 feet long consisting converging mouth entry, honeycomb section 1, fan section, rectangle section, honeycomb section 2, converging diverging section and rectangular exit section. The air flow was generated from the fan inside the tunnel and the air velocity is controlled using variable frequency drive.

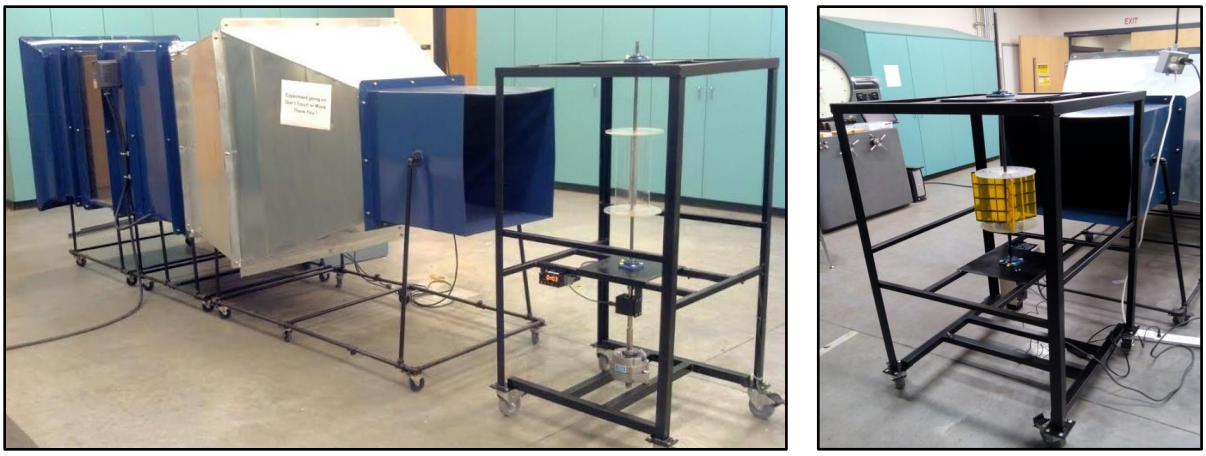

FIGURE 3-12: Complete Experimental Setup of Wind Tunnel

The converging mouth entry designed to easy entry and to maintain uniform flow through the tunnel. First honeycomb section is used to reduce swirling effect and make the flow straight. A variable frequency axial flow fan was used to axial flow fan was used to induce flow through the wind tunnel. Second honeycomb section is used to make flow straight. Converging and diverging section helps to minimize the expansion and contraction loss and to reduce the possibility of flow separation. The exit section was used to make the flow straight and uniform.

3.4.2 Rotor Models

Based on the CFD simulation results, various VAWT scale models were designed and manufactured. Three of the rotors are manufactured: semi-circular, NACA5510 and NACA7510. The models of both NACA5510 and NACA7510 were made of three blades of diameter, d = 5 in and height, H = 10 in. The turbine models were made of wood and film coated with a central shaft of stainless steel of 0.5 in. The blades were 120^0 apart from each other and the overall rotor diameter is D = 10.5 in. The two discs holding the blades were made of acrylic. Fabricated NACA5510 airfoil bladed turbine scale model is shown in Figure 3-7.

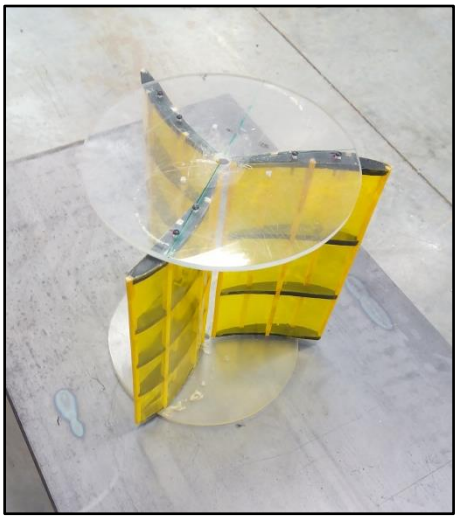

FIGURE 3-13: Fabricated Model of NACA5510 Bladed Rotor

Fabricated semi-circular bladed wind turbines scale model is shown in Figure 3-8. The semi-circular model was made of three semi-cylindrical blades of diameter, d = 4.75 in, and height, H = 11.5 in. The turbine model was made of acrylic without any central shaft. The blades were 120^0 apart from each other and the overall rotor diameter was D = 9.75 in.

FIGURE 3-14: Fabricated Model of Semi Circular Bladed Rotor

These Rotor models were placed in front of the tunnel, with bearing on both side and supporting structures at the same height as the center of the tunnel, between 15 in downstream from the outlet with uniform air flow. These blade models can freely rotate using through shafts and ball bearing collars.

3.4.3 Experimental Procedure

The experiments were carried out at three different wind speeds V = 11.3 m/s, 11.7 m/s and 12 m/s. Wind speed was measured by a handheld anemometer at different location 15 inches from the outlet of wind tunnel around the rotor. The average wind velocity around the rotor was taken into account while calculation.

A dynamic rotary torque transducer (Model: T8 ECO) had been used to measure Torque (T). The rotor was coupled in driving side of the transducer and a constant breaking load was applied on the other side which helps to measure torque. A drop bracket was fabricated that holds the sensor and the break underneath in a location that allows for easy, smooth coupling and roation with the bottom of the main shaft. The sensor itself cannot provide readouts. To

provide said readouts, the DP41-B bench top display was added to the setup as a means of reading real-time torque output via signals transmitted from the compatible torque sensor. The rotational speed of the rotor (N) was measured by non-contact handheld photo tachometer.

3.5 Measured Characteristics

Numerical study provided the drag, lift and torque coefficients. These were directly measured parallel to time of rotation. The force and moment on the blade wall were also directly extracted from the simulation. The angular speed of the rotor was arbitrary calculated to a fixed number for all the models. From the contour we can also see the velocity and pressure profile around the blade.

Angular velocity (ω) was calculated from this measured rotational speed using equation (3.2). These parameters then helped to calculate Tip speed ratio, Reynolds Number, Torque Coefficient and Power Coefficient.

CHAPTER 4

4 Findings of the Study

Numerical findings are the first to find in this study. The change of drag and lift coefficient along with time is the very first characteristics. The overall torque during the steady movement of rotor is extracted and then Torque coefficient, power coefficients are discussed. Experimental results of torque which is directly measured and torque coefficient and power coefficient along with tip speed ratio is discussed for three bladed VAWT for different design. Finally comparison of torque and power coefficients is discussed for different models.

4.1 Numerical Results

Numerically pressure and velocity contours are found directly. Also the drag, lift and moment coefficients are found along with time of rotation. Five different blade shapes have studied for four different wind velocity values.

4.1.1 Pressure Contour

Numerical solution provides the pressure contour for five different models. The negative side of camber or the concave side of circular blade has lower pressure than the positive camber or convex side of blade. This creates the positive and negative pressure region and the difference causes the rotation. After 5 seconds of rotation at various wind speed the pressure around the rotor blades are little different.

The higher wind speed creates more negative pressure at the negative camber. Figure 4-1 shows the characteristics for NACA 5510 profile.

i)

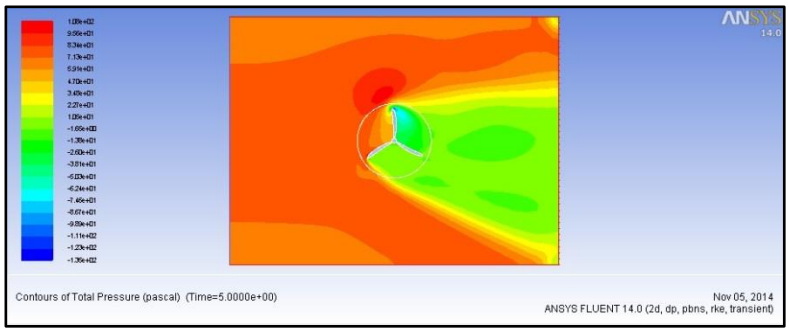

ii)

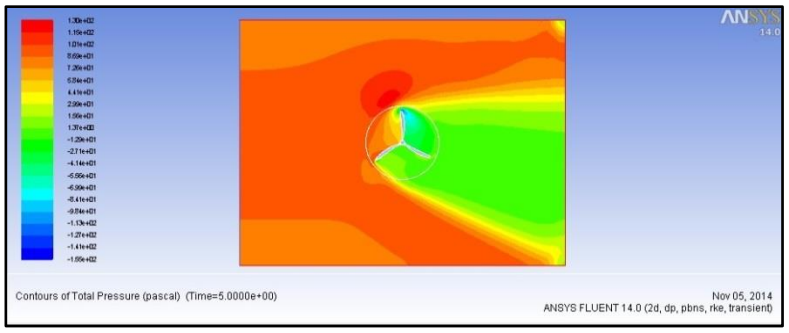

iii)

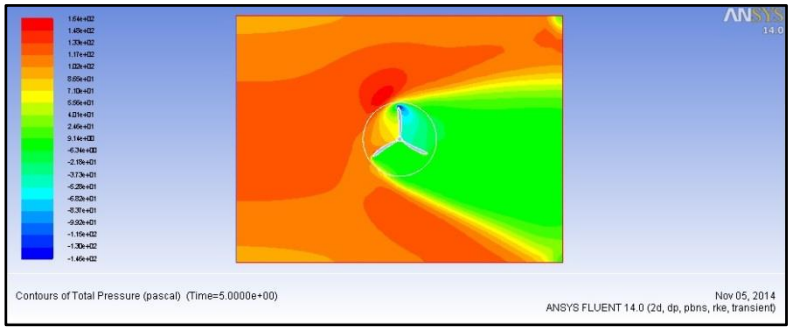

iv)

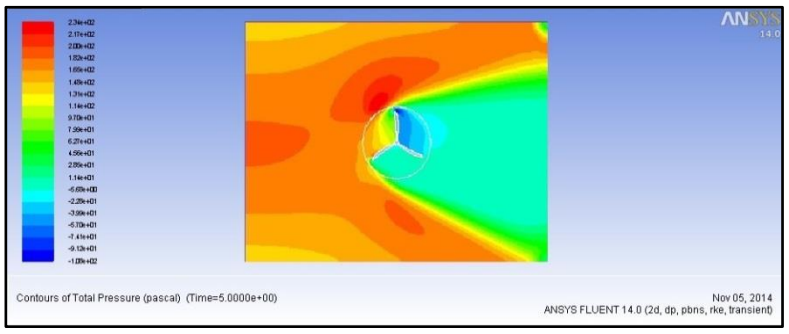

FIGURE 4-1: Pressure Contour around NACA5510 at TSR i) 0.226, ii) 0.247, iii) 0.271 and iv) 0.301

Figure 4-2 shows the characteristics for NACA 7510 profile. NACA7510 provides lesser maximum pressure and more minimum pressure than NACA5510

i)

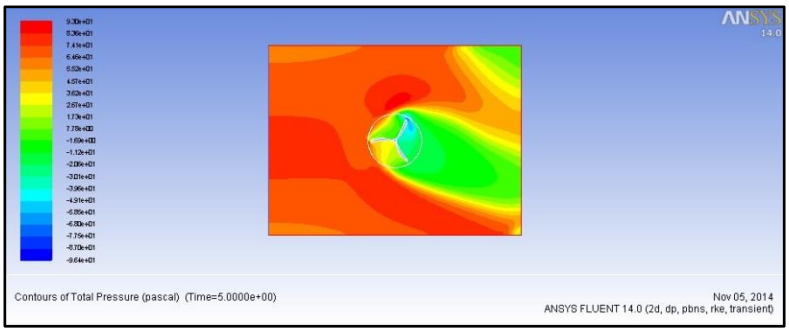

ii)

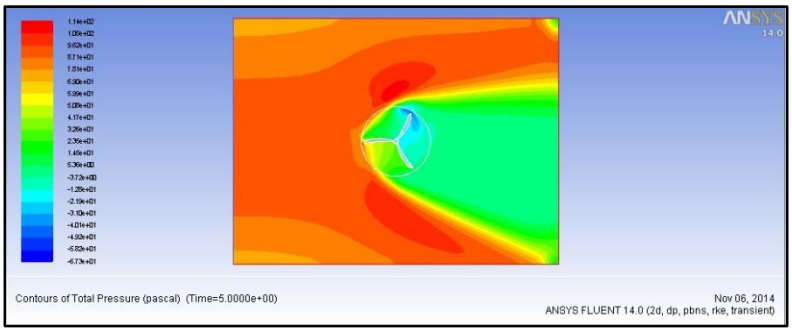

iii)

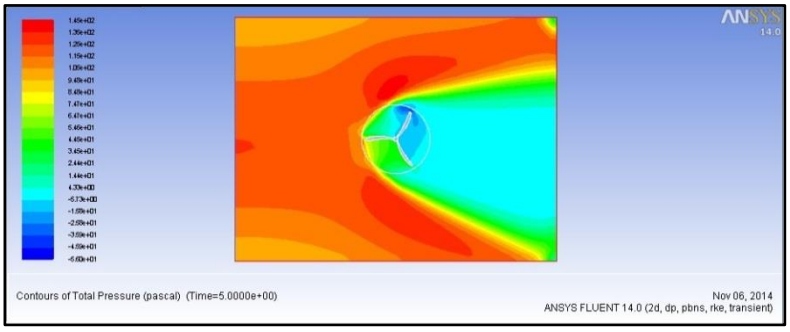

iv)

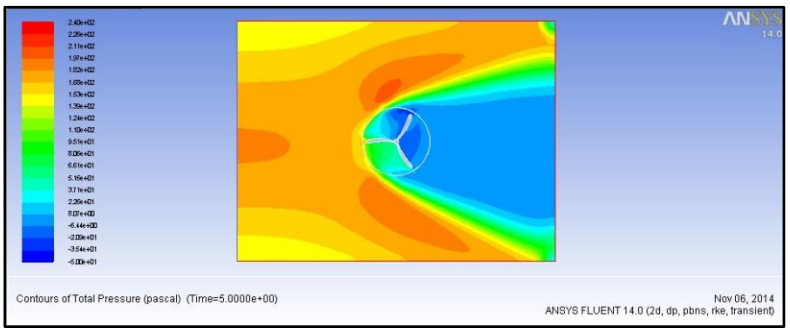

FIGURE 4-2: Pressure Contour around NACA7510 at TSR i) 0.226, ii) 0.247, iii) 0.271 and iv) 0.301

Figure 4-3 shows the characteristics for NACA 9510 profile. NACA9510 shows a same pressure profile like NACA 7510.

i)

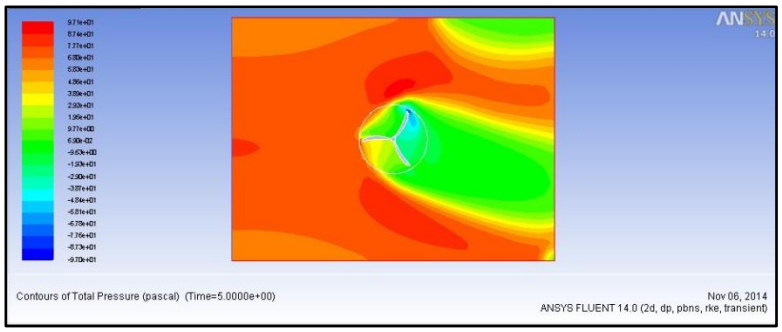

ii)

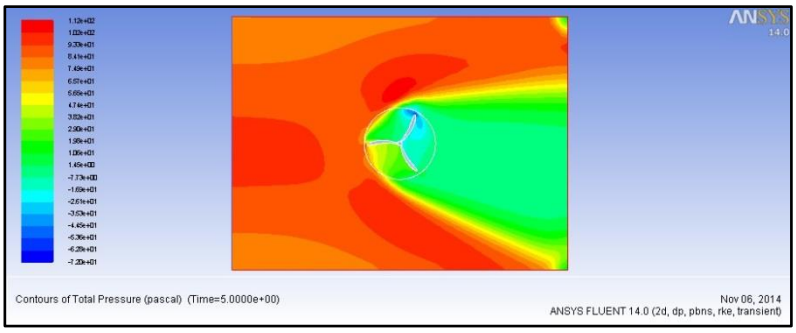

iii)

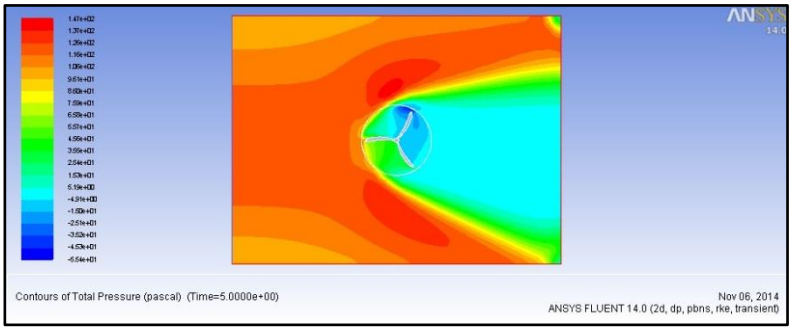

iv)

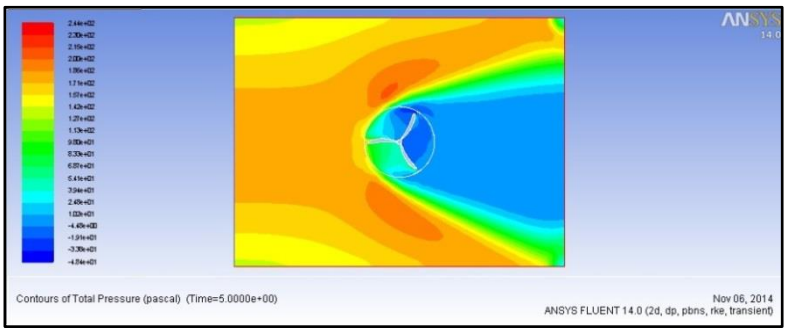

FIGURE 4-3: Pressure Contour around NACA9510 at TSR i) 0.226, ii) 0.247, iii) 0.271 and iv) 0.301

Unlike NACA airfoil, quarter-circular blade shows almost similar pressure profile for different TSR. The opposite side of turbine produces negative pressure. It produces less minimum pressure

i)

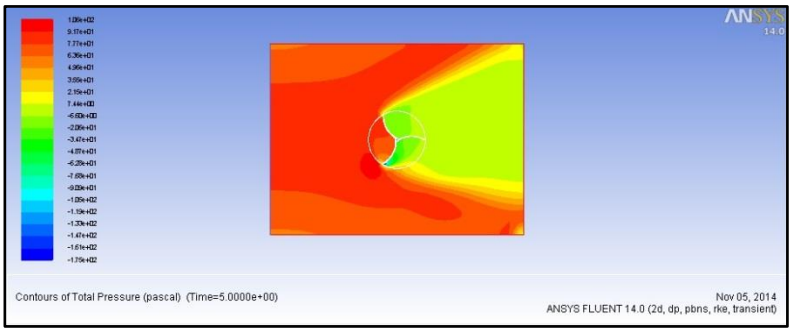

ii)

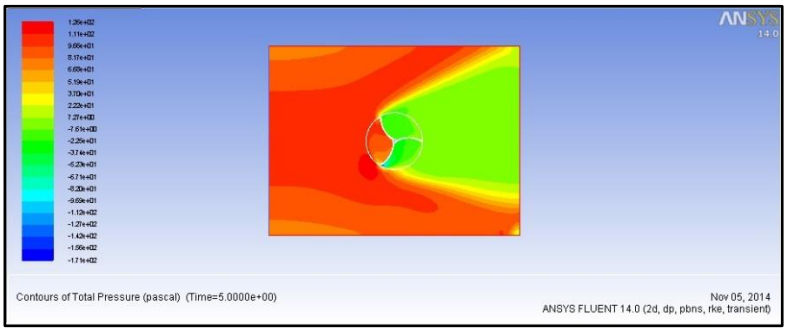

iii)

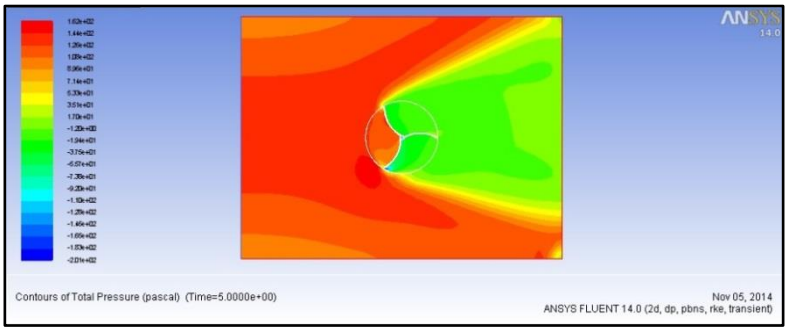

iv)

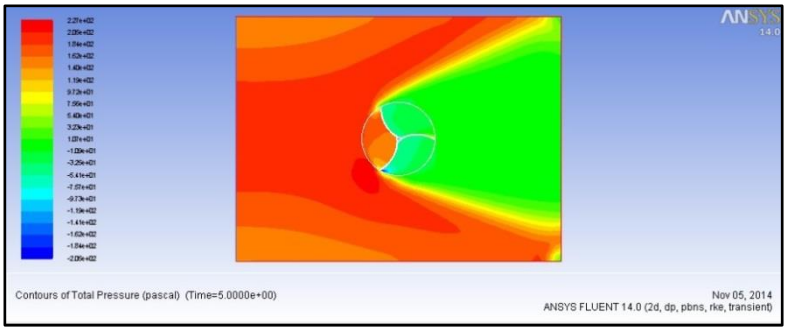

FIGURE 4-4: Pressure Contour around Quarter-Circular at TSR i) 0.226, ii) 0.247, iii) 0.271 and iv) 0.301

Semi-circular bladed rotor behaves same as quarter-circular bladed rotor. The only difference is it produces more pressure difference.

i)

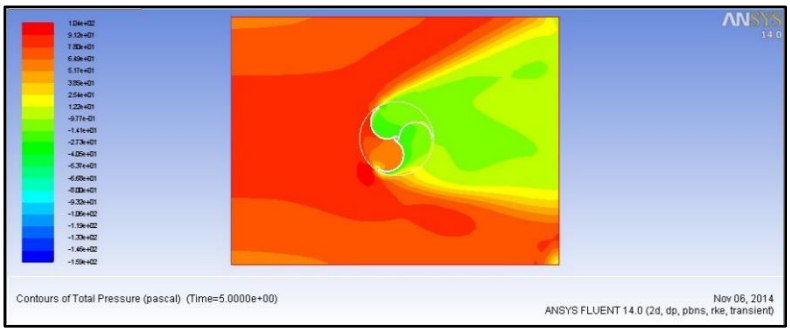

ii)

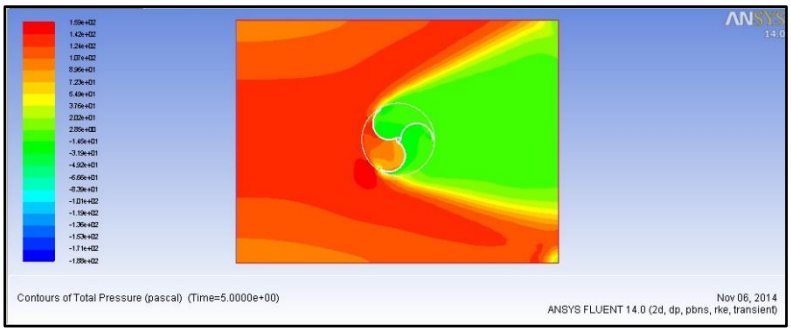

iii)

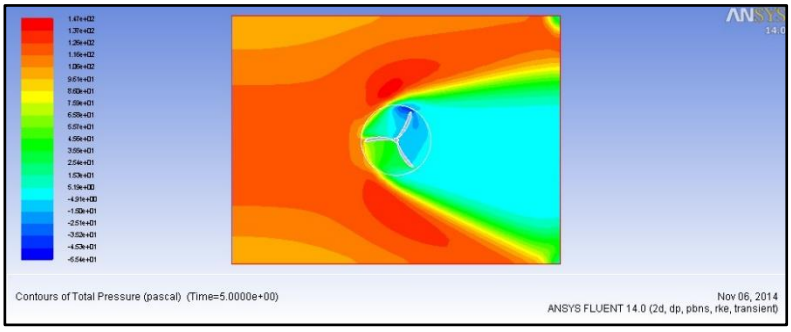

iv)

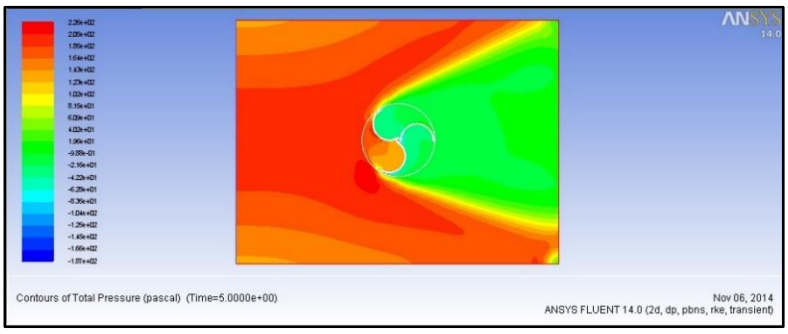

FIGURE 4-5: Pressure Contour around Semi-Circular Rotor at TSR i) 0.226, ii) 0.247, iii) 0.271 and iv)0.301

The comparisons of highest and lowest pressure are shown in the following table:

	NACA5510		NACA7510		NACA9510		Semi-circular		Quarter-circular	
TSR	Max	Min	Max	Min	Max	Min	Max	Min	Max	Min
	Pascal									
0.226	107.7	-135.3	93	-96.4	97.1	-96.4	104.4	-159	105.8	-174.1
0.247	129.7	-155.4	114.4	-67.3	111.6	-67.3	125	-162	126.3	-171.3
0.271	163.9	-145.6	145.1	-46	146.6	-46	159	-188	162.2	-200.9
0.301	233.8	-108.3	240.0	-50	240.1	-50	225.8	-186.6	226.9	-205.4

TABLE 1: Max and Min Pressure after 5 Sec. of Rotation for All the Rotor Models at Different TSR

The outcome of the pressure contour after 5 seconds of rotation is almost similar for all the models. The pressure profiles around the blades show that, the change for all the models produce same picture. The highest and lowest pressure as well as the pressure difference of the rotors varies each time.

4.1.2 Velocity Contour

Velocity contour for five different models at four different tip speed ratio are compared. Once the wind comes near the rotor the velocity magnitude starts to decrease. The velocity remains always lowest at the trailing edge of the blade. Then after hitting the wind at the blade the wind also produces some angular velocity and start to gain the velocity again.

In general the higher velocity region is displayed at the leading edge of the blade specially at the blade which is on the pressure side. The back of the rotor side always creates a vacuum and remains at lowest velocity.

i)

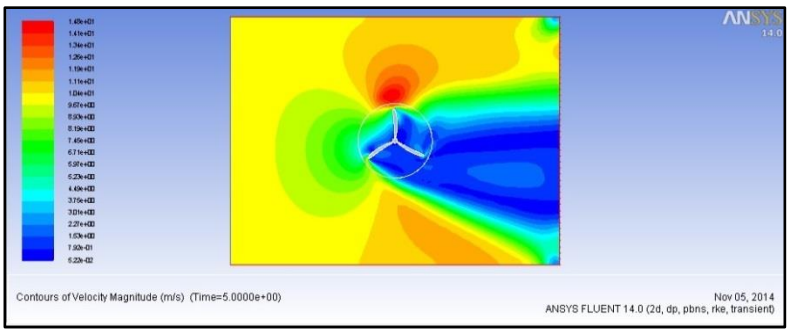

ii)

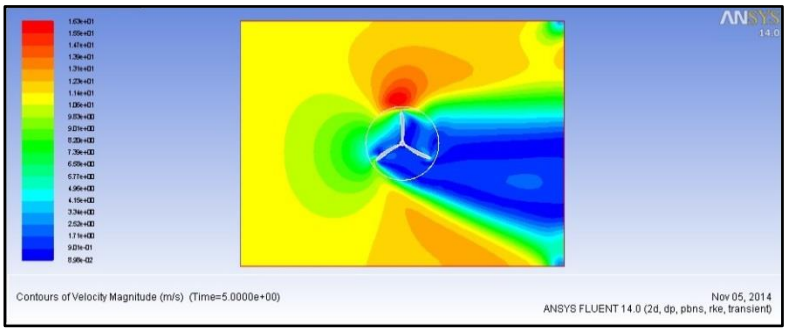

iii)

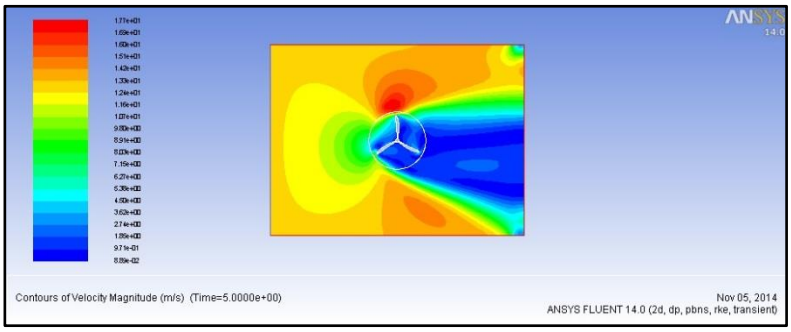

iv)

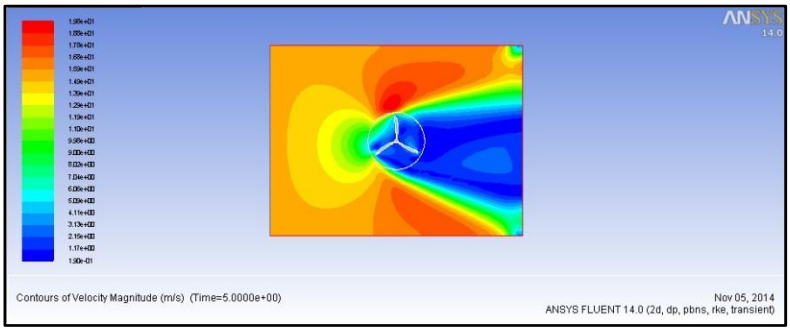

FIGURE 4-6: Velocity Contour around NACA5510 at TSR i) 0.226, ii) 0.247, iii) 0.271 and iv) 0.301

i)

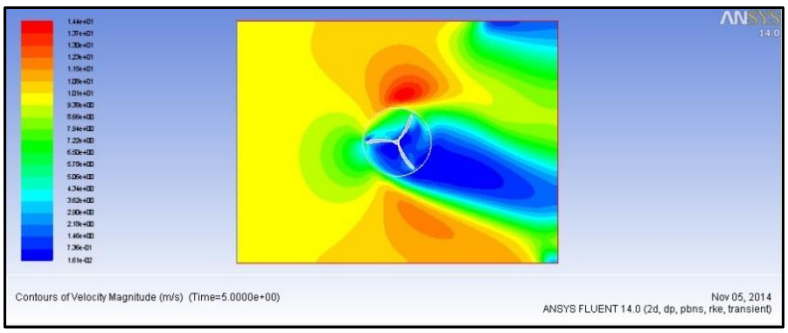

ii)

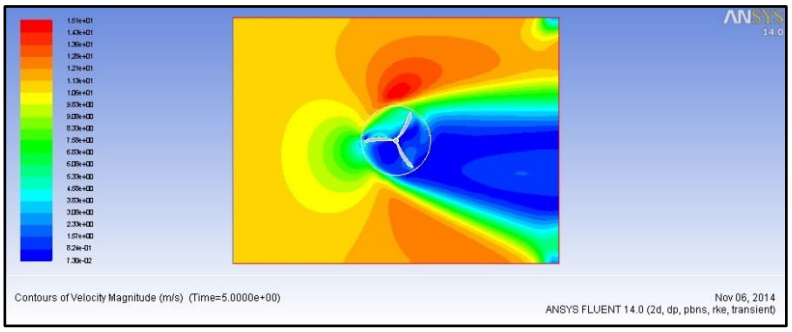

iii)

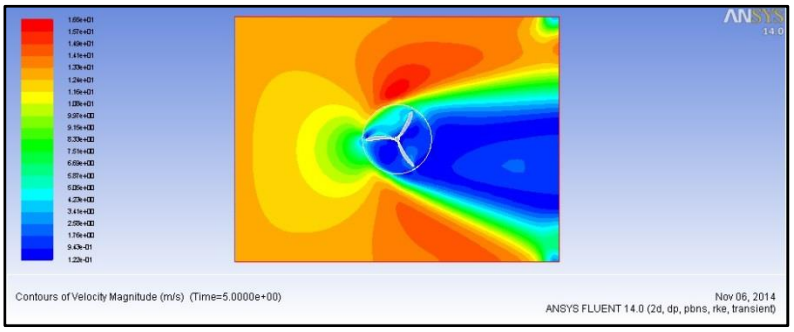

iv)

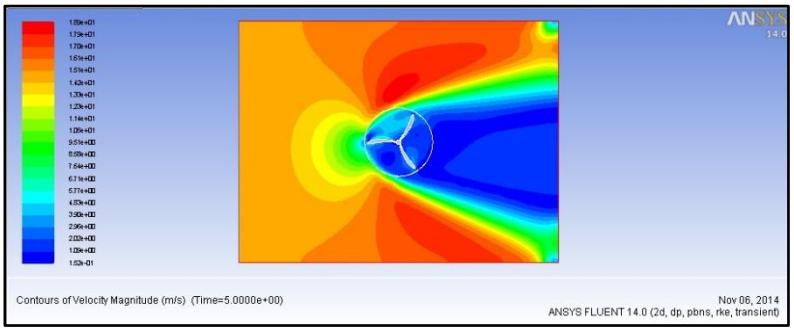

FIGURE 4-7: Velocity Contour around NACA7510 at TSR i) 0.226, ii) 0.247, iii) 0.271 and iv) 0.301

i)

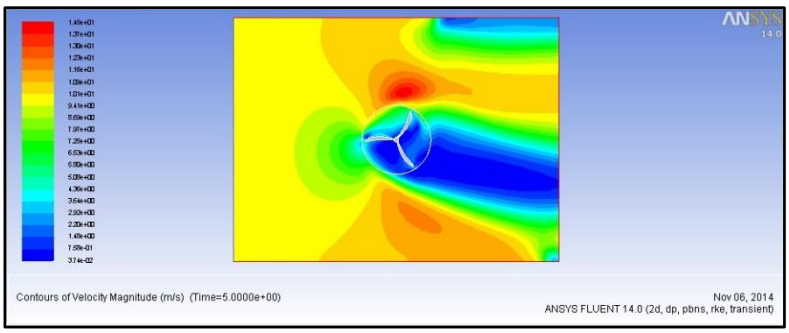

ii)

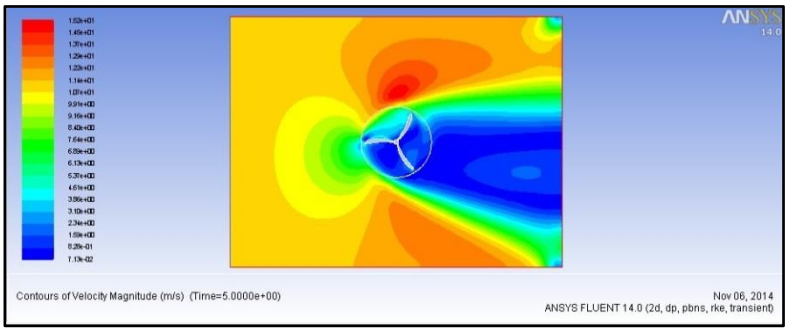

iii)

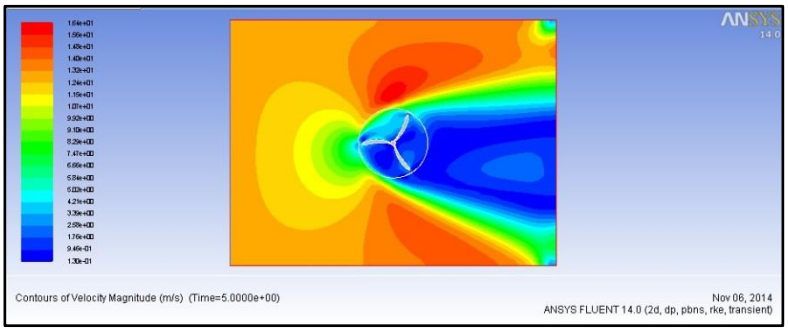

iv)

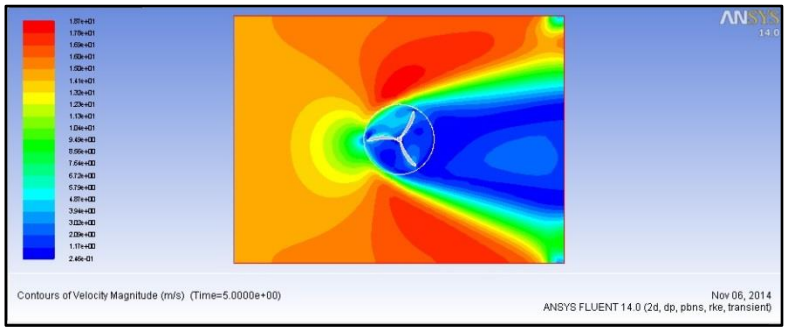

FIGURE 4-8 Velocity Contour around NACA9510 at TSR i) 0.226, ii) 0.247, iii) 0.271 and iv) 0.301

i)

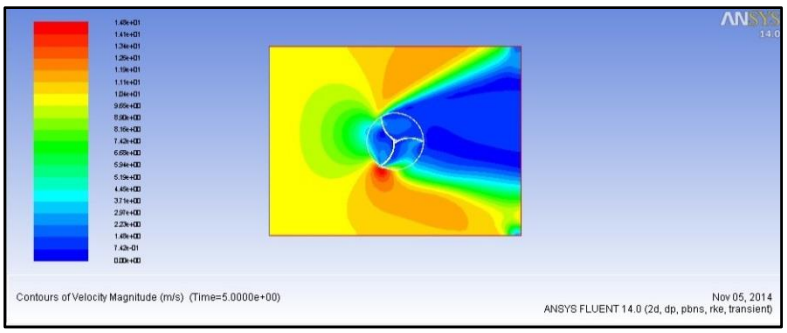

ii)

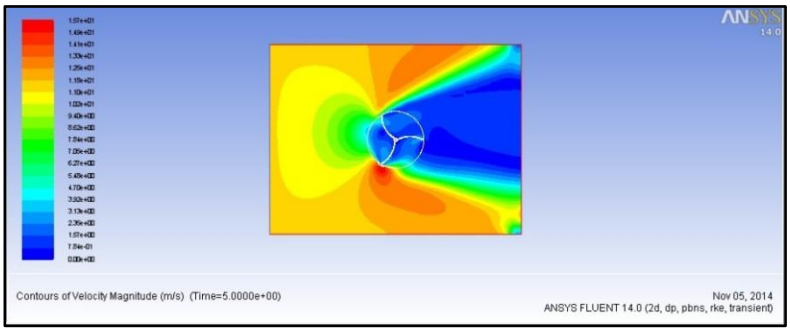

iii)

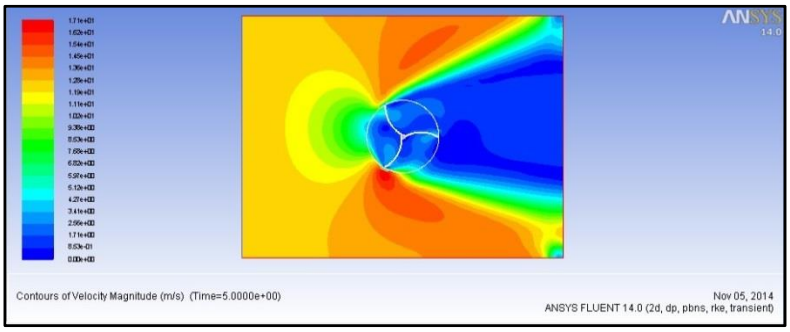

iv)

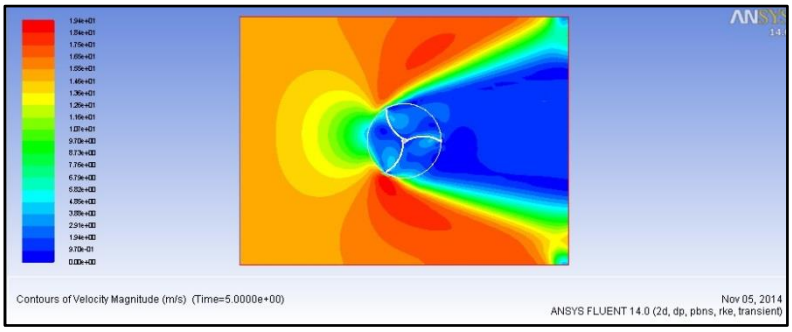

FIGURE 4-9: Velocity Contour around Quarter-Circular at TSR i) 0.226, ii) 0.247, iii) 0.271 and iv) 0.301

i)

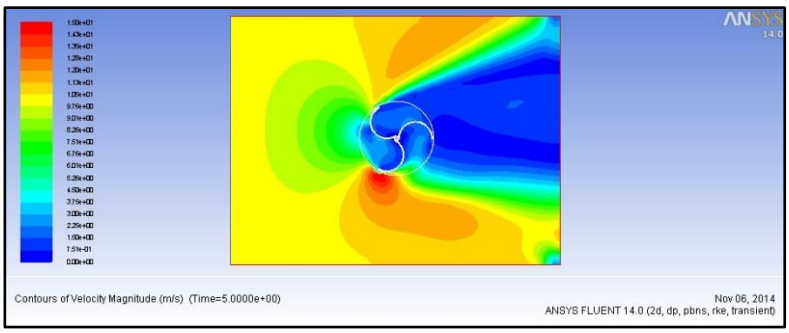

ii)

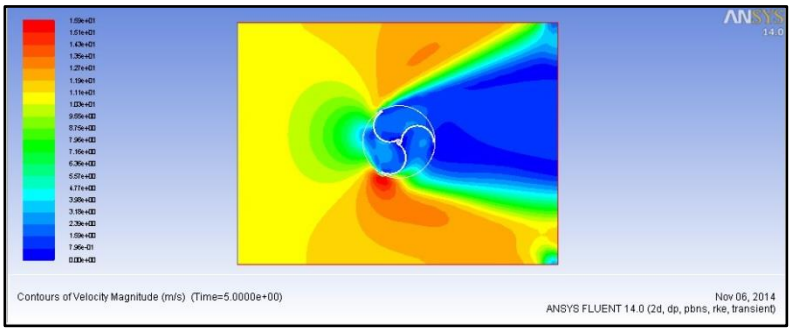

iii)

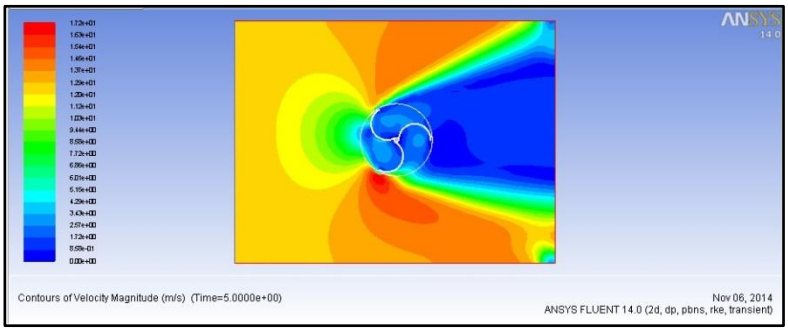

iv)

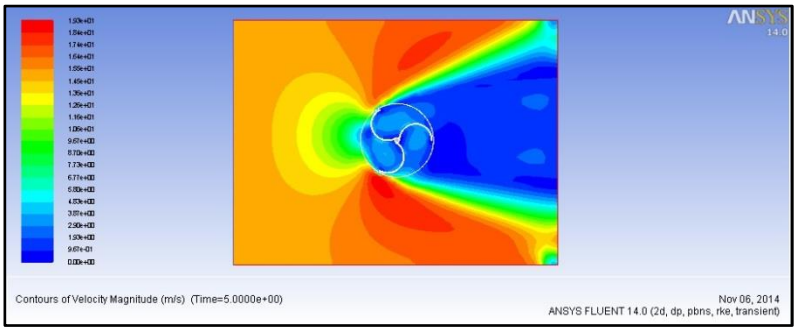

FIGURE 4-10: Velocity Contour around Semi-Circular at TSR i) 0.226, ii) 0.247, iii) 0.271 and iv) 0.301

Contours of Velocity magnitude for all the rotors at different TSR are shown in Figures 4-6 to 4-10. The table-2 below shows the comparison of maximum and minimum velocity among those five models. The outcome of velocity profile after 5 seconds of rotation for each Tip Speed Ratio looks almost similar. They have almost similar maximum and minimum velocity. Increase of wind velocity also increases the velocity around the rotor and they are showing the same pattern of velocity profile and increment.

The only difference for airfoil and non-airfoil is non-airfoil produces 0 m/s, which means complete vacuum at the back of rotor when airfoil has some very little amount of flow.

	NACA5510		NACA7510		NACA9510		Semi-circular		Quarter-circular	
TSR	Max	Min	Max	Min	Max	Min	Max	Min	Max	Min
	m/s									
0.226	14.85	0.05	14.4	0.02	14.5	0.04	15.01	0	14.85	0
0.247	16.3	0.09	15.1	0.07	15.2	0.07	15.9	0	15.7	0
0.271	17.7	0.09	16.5	0.12	16.4	0.13	17.2	0	17.06	0
0.301	19.8	0.19	18.9	0.15	18.7	0.25	19.3	0	19.4	0

TABLE 2: Max and Min Velocity after 5 Sec. of Rotation for All the Rotor Models at Different TSR

4.1.3 Drag Coefficient

Drag coefficient (C_d) changes with the change of time and rotation of turbine. The starting drag coefficient changes sharply towards positive from negative and then the curve shows a sinusoidal behavior. With the change of angle of rotation the curve moves from positive to negative and to positive again. This drag coefficient is the key factor that produces thrust on the blade which eventually helps to rotate the wind turbine.

Drag coefficient vs. Angle of Rotation

The drag coefficient (C_d) of each blade and combined blade effect of three bladed Savonius wind turbine model variation with the change in rotor angle (θ) is shown in Figure 4.11. The drag coefficient here is displayed after the start, so it shows almost uniform movement. The plot is displayed at 15° interval from 0° to 360°. Drag coefficient increases with the increase of rotor angle and then decreases with the increase of angle.

i)

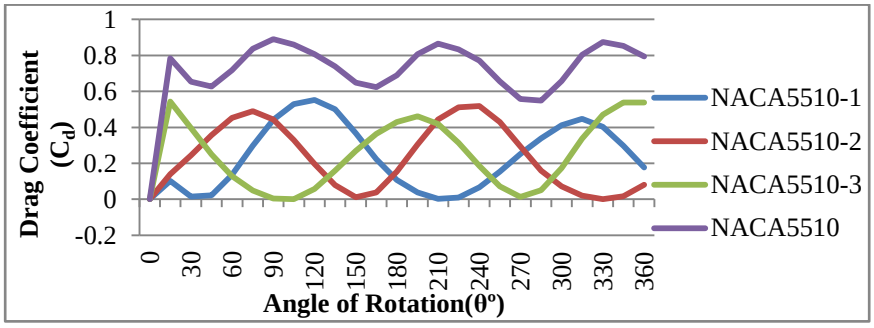

ii)

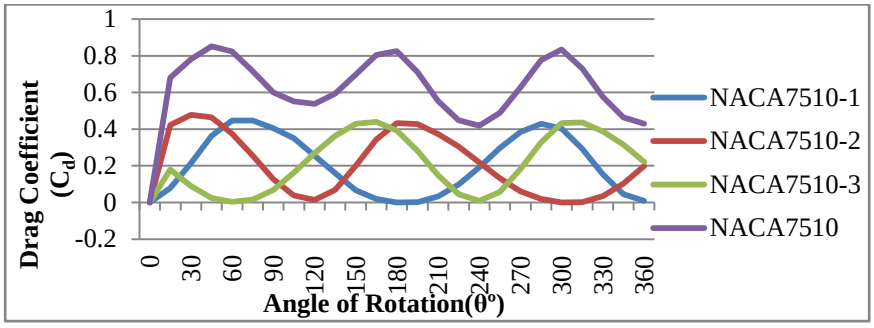

iii)

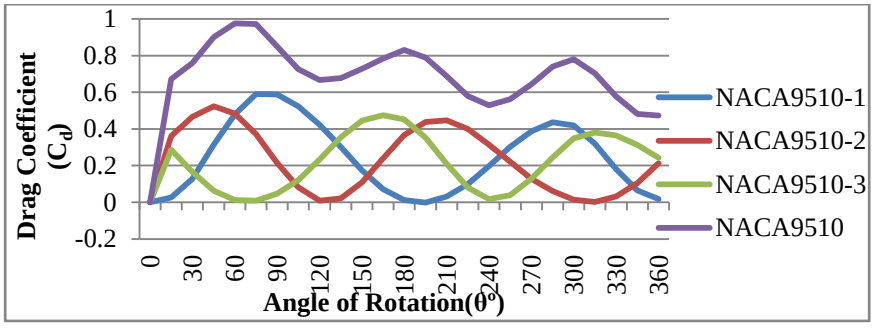

iv)

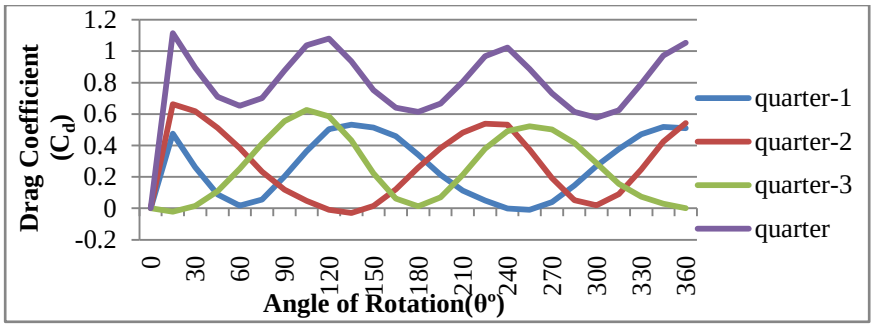

v)

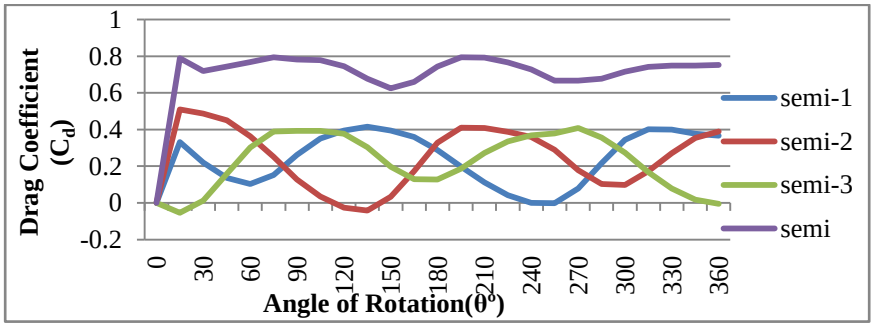

FIGURE 4-11: Drag Coefficient (C_d) vs. Angle of rotation (θ) for Single Blade and Three Blades Combined Effect at TSR 0.226 for Five Models

Semi Circular bladed model shows less oscillation for combined drag coefficient, while the highest drag coefficient is displayed for quarter-circular bladed rotor.

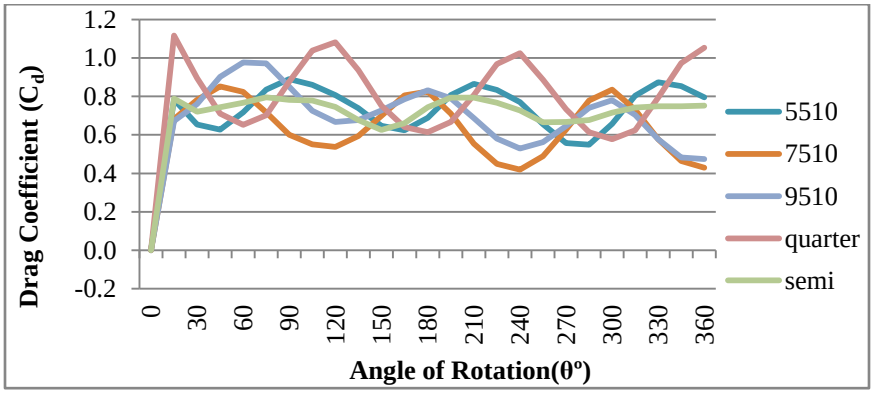

FIGURE 4-12: Drag Coefficient (C_d) vs. Angle of rotation (θ) for Three Blades Combined Effect at TSR 0.226 for Five Models

Drag coefficient vs. Time of Rotation

For NACA5510 model, the starting drag coefficient is lowest for highest TSR and it is more for lower TSR. The models are rotated for 5 seconds but after .08 seconds the curve is not showing any more special movement. Figure 4-13 shows the drag coefficient for four different TSR for 0.5 seconds and magnified view after 0.1 second for NACA 5510.

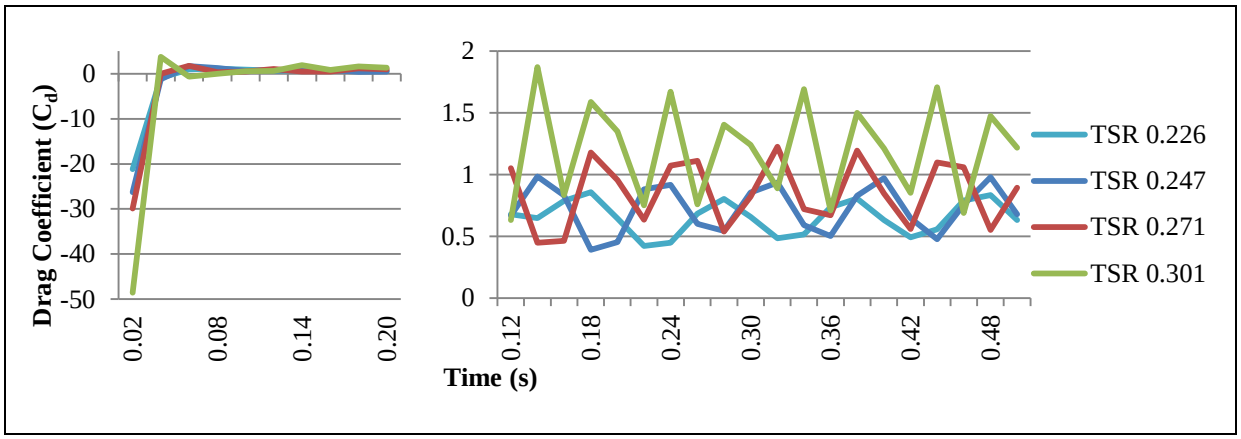

FIGURE 4-13: Drag Coefficient (C_d) vs. Time for NACA5510 for Different TSR

For NACA7510 model, the starting drag coefficient is lowest for highest TSR. Figure 4-14 shows the drag coefficient for four different TSR for 0.5 seconds and magnified view after 0.1 second for NACA 7510 model.

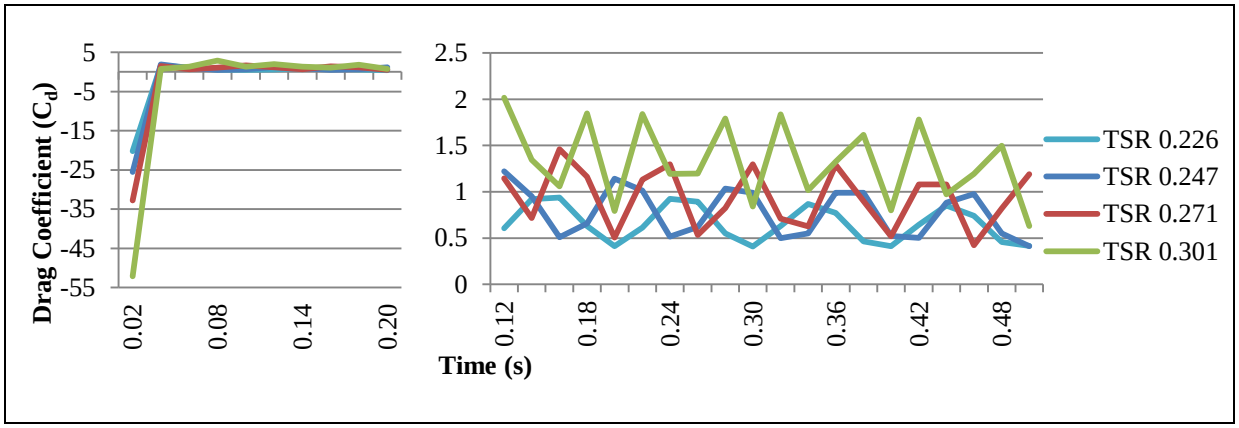

FIGURE 4-14: Drag Coefficient (C_d) vs. Time for NACA7510 for Different TSR

For NACA9510 model also demonstrate the same behavior. Figure 4-15 shows the drag coefficient for four different TSR for 0.5 seconds and magnified view after 0.1 second.

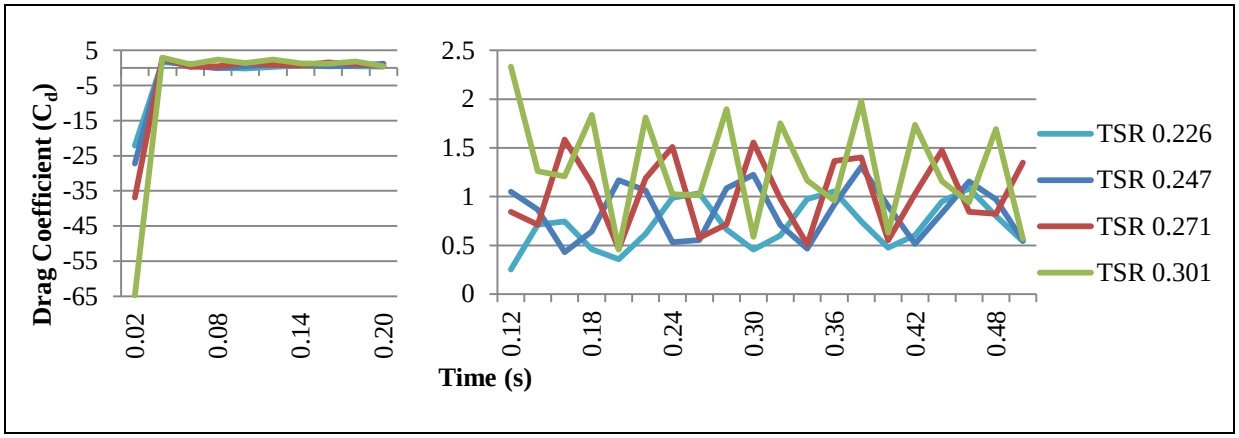

FIGURE 4-15: Drag Coefficient (C_d) vs. Time for NACA9510 for Different TSR

Quarter Circular bladed rotor almost showing the same behavior but TSR 0.301 provides negative coefficient up to 0.10 second which is unlike before. Figure 4-16 shows the drag coefficient for four different TSR for 0.5 seconds and magnified view after 0.1 second.

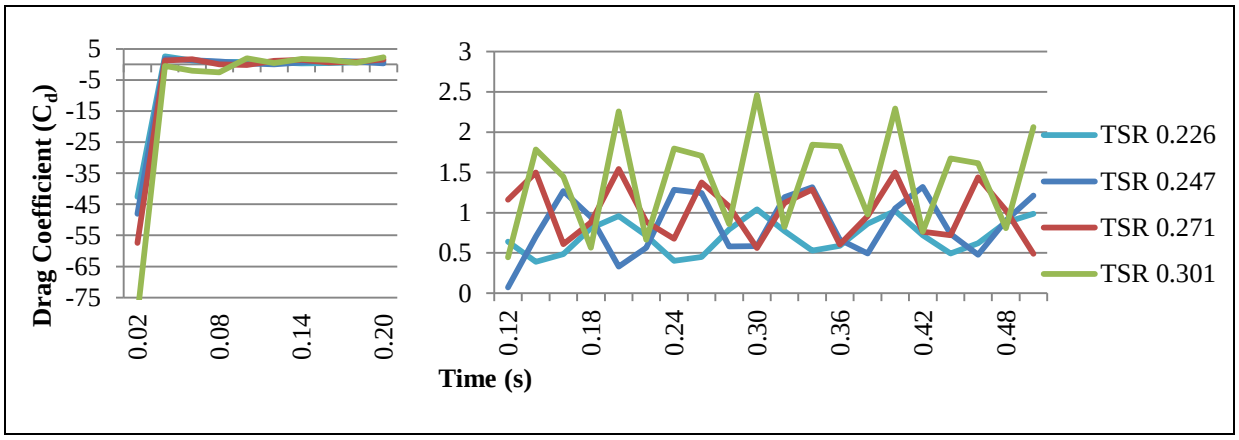

FIGURE 4-16: Drag Coefficient (C_d) vs. Time for Quarter-Circular Rotor for Different TSR

Finally Semi Circular bladed rotor shows a little different behavior. TSR 0.271 had higher drag coefficient for first few seconds. And then the coefficient shows similar behavior like before. Figure 4-17 shows the drag coefficient for four different TSR for 0.5 seconds and magnified view after 0.1 second.

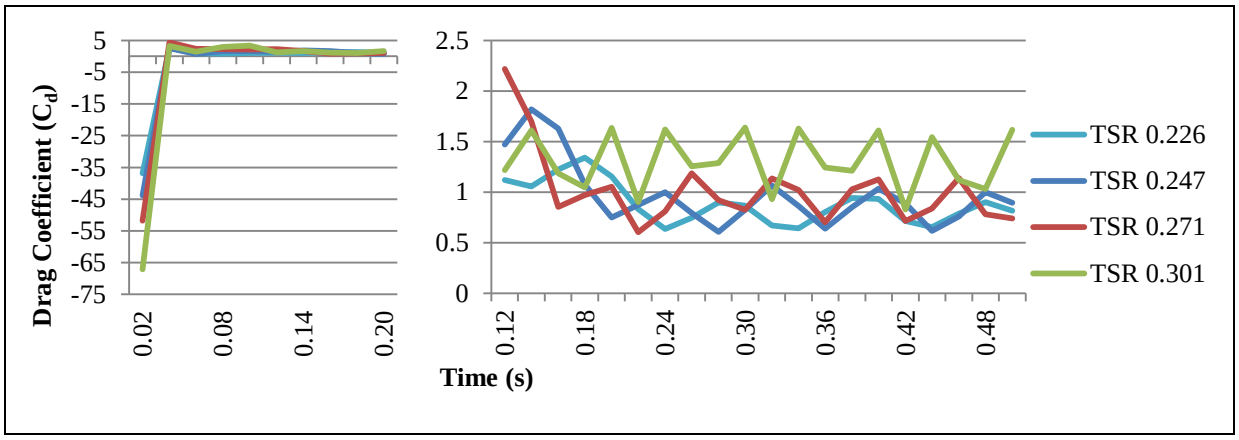

FIGURE 4-17: Drag Coefficient (C_d) vs. Time for Semi-Circular rotor for Different TSR

The average drag coefficients of five different models are shown at figure 4-18. For different TSR, all the drag coefficients are averaged and then plotted. NACA5510 rotor always produce highest drag coefficient. Increase of camber number decreases the drag coefficient. For circular blades, the drag coefficient increases when the TSR also increases.

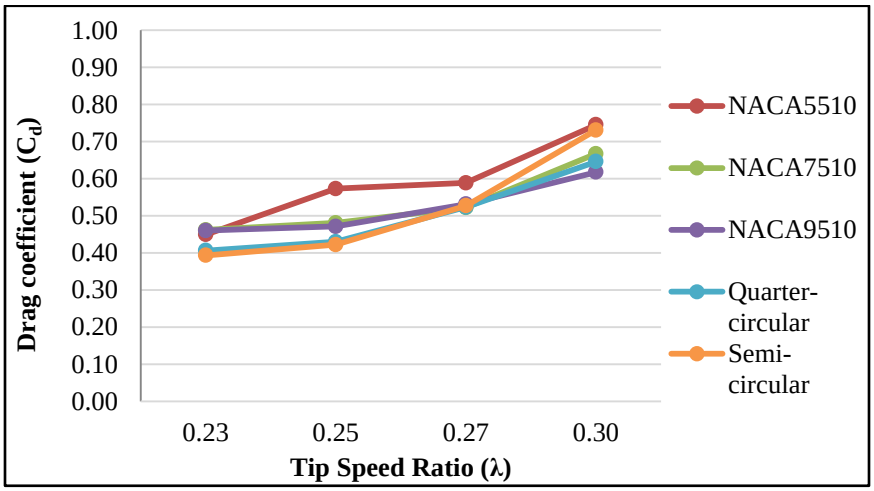

FIGURE 4-18: Average Drag Coefficient (C_d) vs. Tip Speed Ratio (λ) for Different Blades

4.1.4 Lift Coefficient

Lift Coefficient (C_l) is another important characteristic. For the airfoil lift force also helps to create a negative pressure at the negative camber this will eventually increases the positive drag.

Lift coefficient vs. Angle of Rotation

The lift coefficient (C_l) of each blade and combined blade effect of three bladed wind turbine model variation with the change in rotor angle (θ) is shown in Figure 4.19. The lift coefficient here is displayed while rotor was at almost uniform movement.

i)

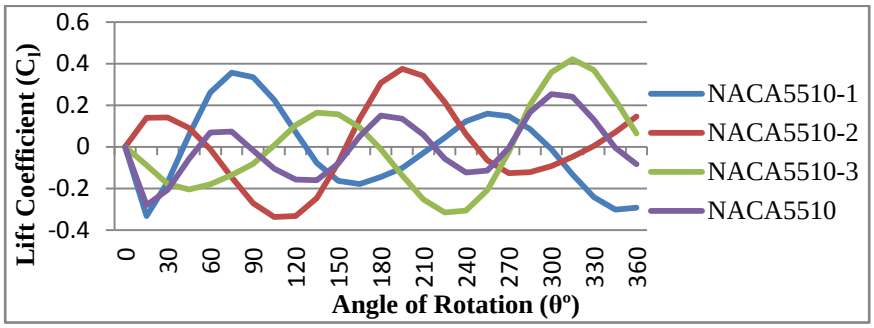

ii)

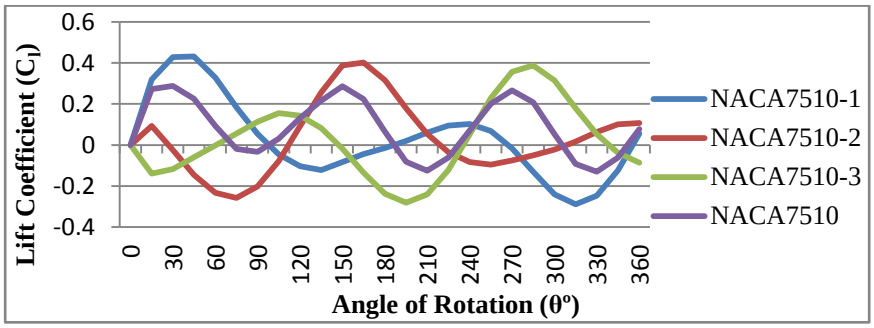

iii)

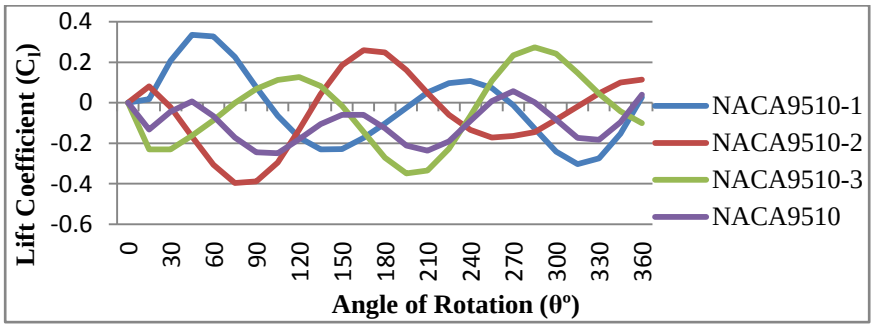

iv)

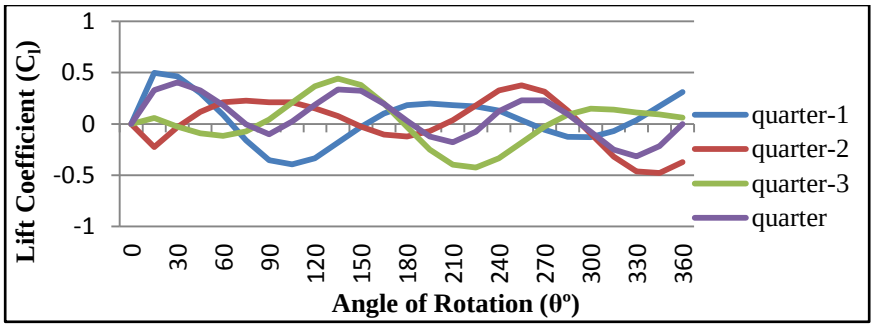

v)

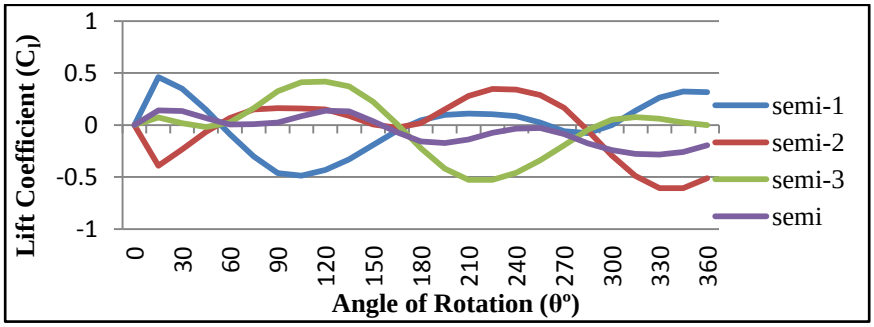

FIGURE 4-19: Lift Coefficient (C_l) vs. Angle of rotation (θ) for Single Blade and Three Blades Combined Effect at TSR 0.226 for Five Models

The plot is displayed at 15° interval from 0° to 360°. Figure 4-20 shows the combined effect of three blades on lift coefficient. Semi Circular bladed model shows less oscillation for combined lift coefficient. NACA7510 shows the overall highest lift coefficient.

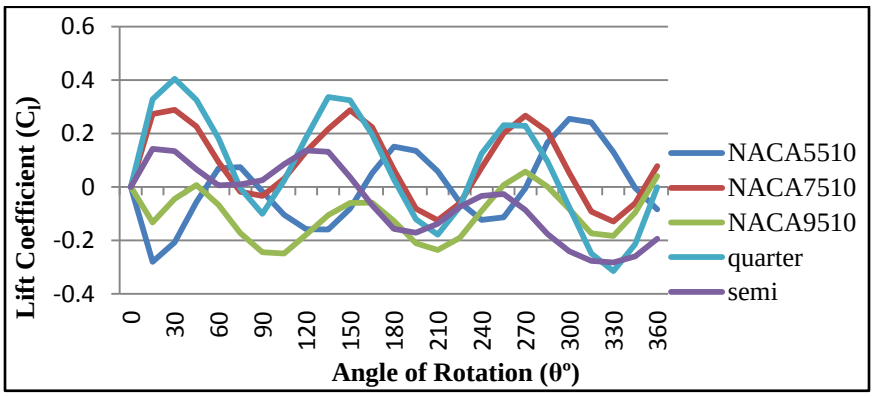

FIGURE 4-20: Lift Coefficient (C_l) vs. Angle of rotation (θ) for Three Blades Combined Effect at TSR 0.226 for Five Models

Lift coefficient vs. Time of Rotation

The starting lift coefficients changes sharply from positive to negative and then the curve shows a sinusoidal behavior.

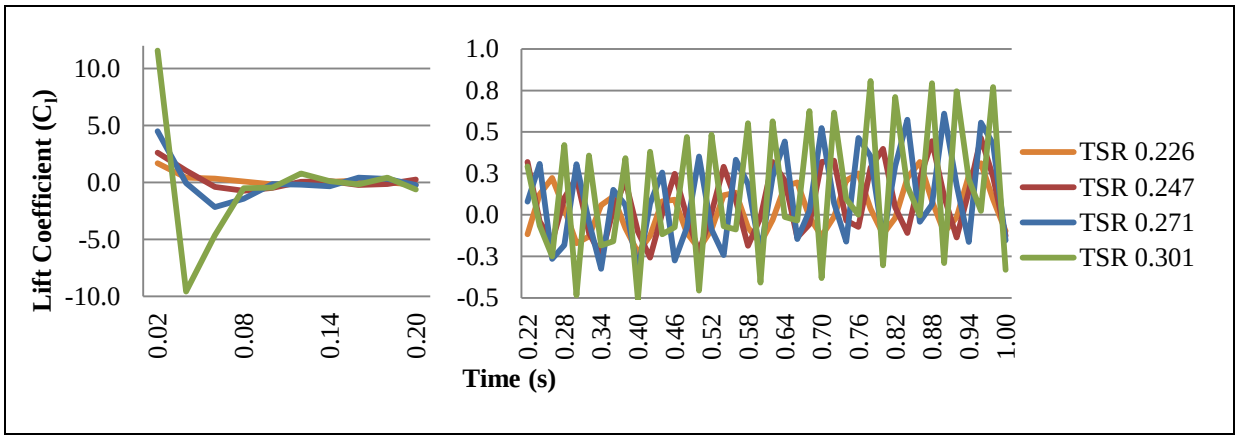

FIGURE 4-21: Lift Coefficient (C_l) vs. Time for NACA5510 for Different TSR

For NACA5510 model, the starting lift coefficient is highest for higher TSR and it is less for lower TSR. The models are rotated for 5 seconds but after 0.1 seconds the curves are almost steady but after 1.0 second there is little wave shown for a single TSR.

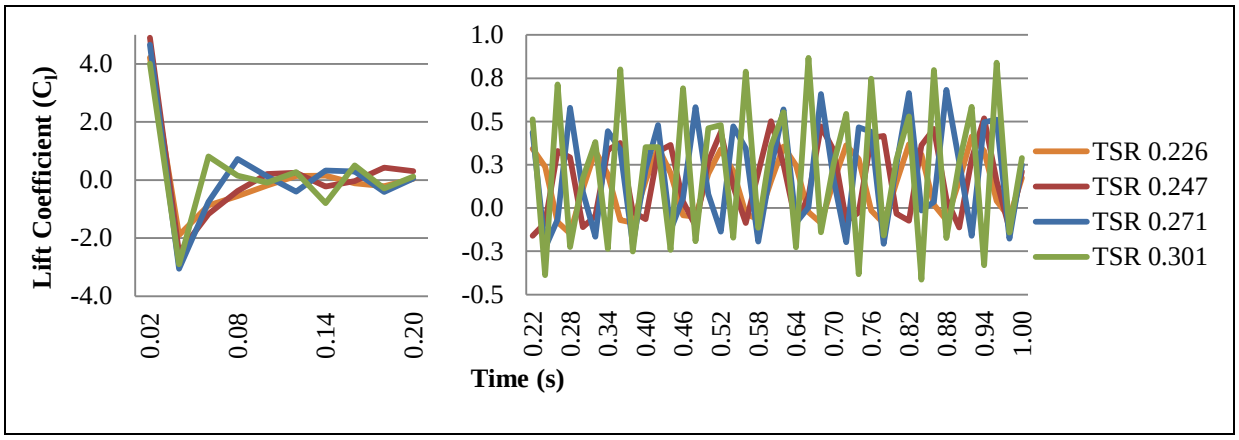

FIGURE 4-22: Lift Coefficient (C_l) vs. Time for NACA7510 for Different TSR

Unlike NACA5510; NACA7510 model shows steady behavior just after 0.1 sec. Higher TSR shows higher lift coefficient. Figure 4-22 shows the lift coefficient for four different TSR.

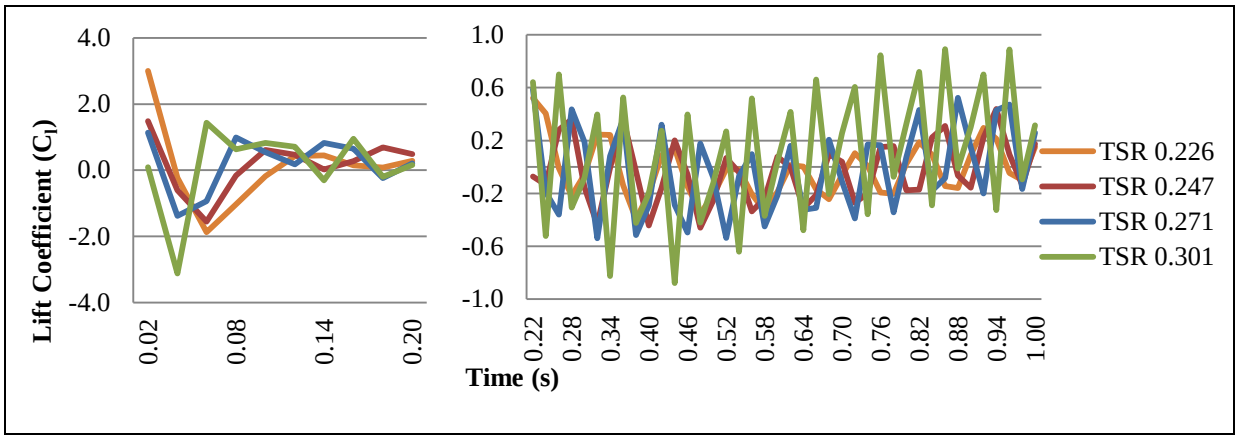

FIGURE 4-23: Lift Coefficient (C_l) vs. Time for NACA9510 for Different TSR

NACA9510 model shows completely different behavior than previous two models. The starting lift coefficient is highest for lower TSR and it is less for higher TSR. TSR 0.301 shows little unsteady behavior until 1.0 second. Figure 4-23 shows the lift coefficient for four different TSR for 1.0 second.

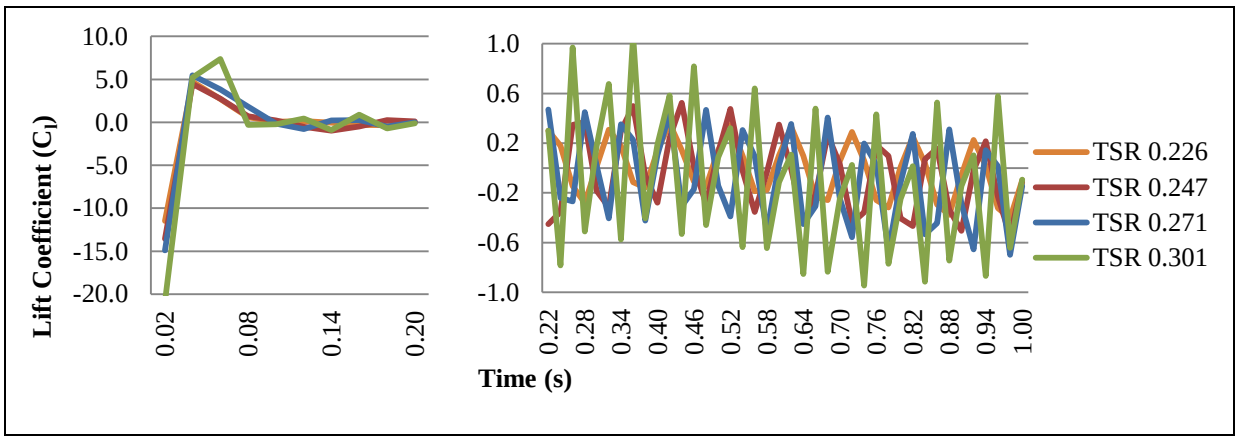

FIGURE 4-24: Lift Coefficient (C_l) vs. Time for Quarter-Circular Rotor for Different TSR

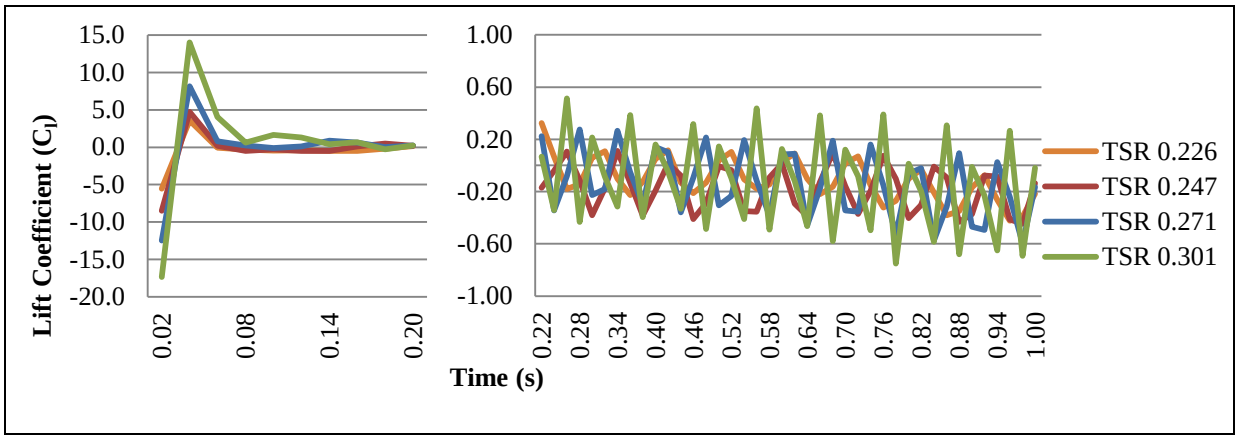

FIGURE 4-25: Lift Coefficient (C_l) vs. Time for Semi-Circular Rotor for Different TSR

For both circular shaped bladed rotor the starting lift coefficient is very low and jumped to positive and after 0.2 seconds the behavior remains steady. The higher TSR has higher lift coefficient. Figure 4-16 and 17 shows the behavior.

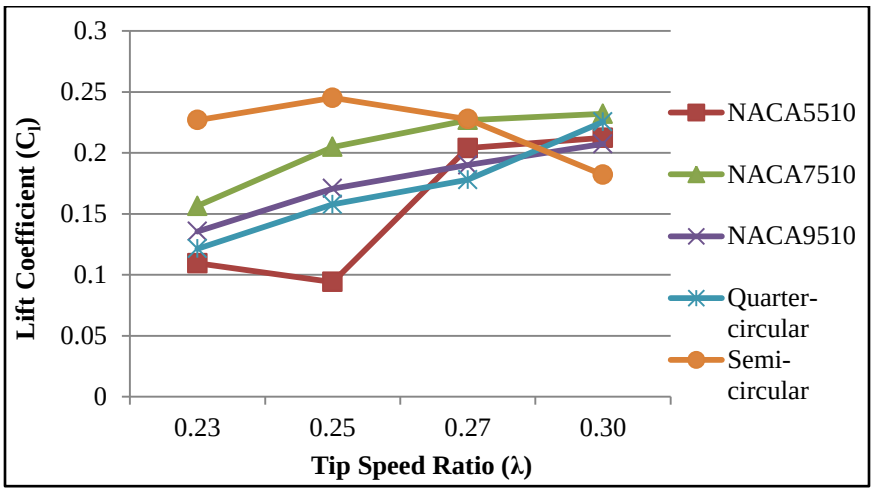

FIGURE 4-26: Average Lift Coefficient (C_l) vs. Tip Speed Ratio (λ) for Different Blades

For different TSR, all the lift coefficients of five different models are averaged and then plotted; shown in figure 4-18. NACA7510 rotor produce better lift coefficient.

Semi-circular rotor shows negative tendency for higher TSR. But Quarter circular rotor shows same behavior like the airfoils. Around TSR 0.301 seems to be the optimum point.

4.1.5 Torque Coefficient

The torque is measured from the numerical solution. This torque is measured at a certain point of the rotation. As the torque is always changed for rotational component, so it is assumed that the combined effect is averaged when to rotor starts to show steady movement for steady wind velocity.

Torque coefficient vs. Angle of Rotation

The torque coefficient (Cq) of each blade and combined blade effect of three bladed wind turbine model variation with the change in rotor angle (θ) is shown in Figure 4.27. The torque coefficient here is displayed while rotor was at almost uniform movement.

i)

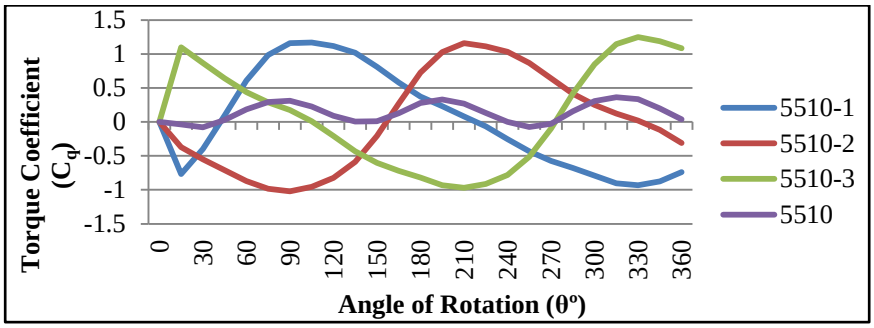

ii)

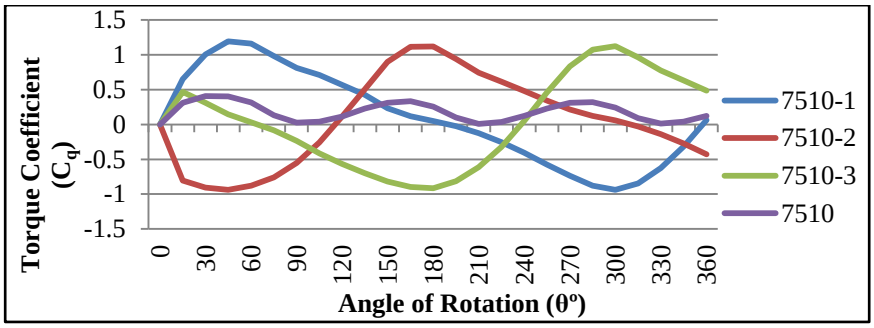

iii)

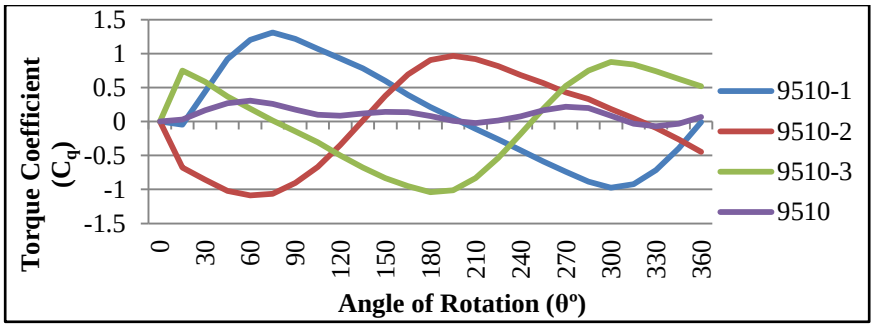

iv)

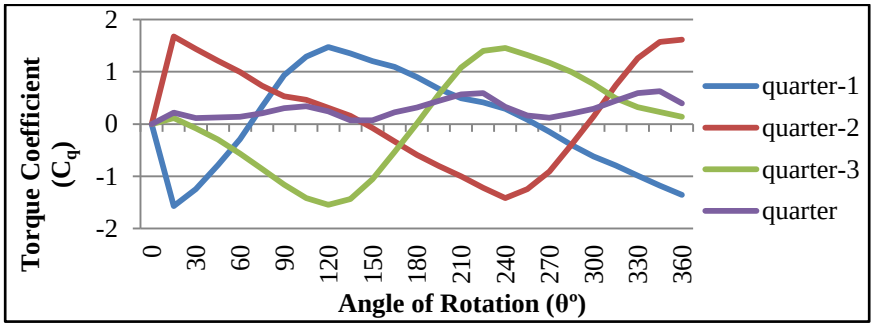

v)

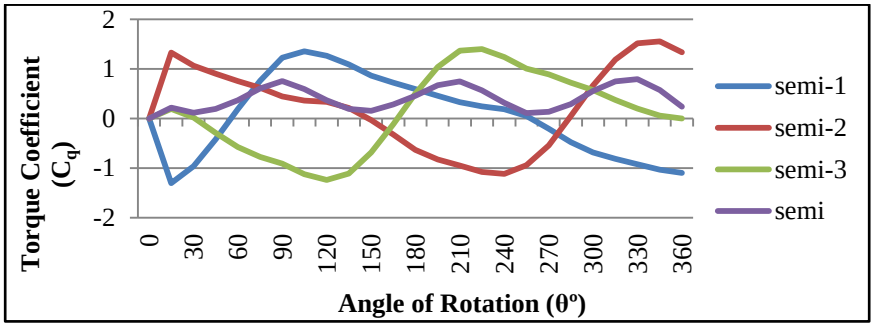

FIGURE 4-27: Torque Coefficient (C_q) vs. Angle of rotation (θ) for Single Blade and Three Blades Combined Effect at TSR 0.226 for Five Models

The plot is displayed at 15° interval from 0° to 360°. Figure 4-28 shows the combined effect of three blades on torque coefficient. Semi Circular bladed model shows the highest torque coefficient. While NACA7510 shows the better coefficient among the airfoils.

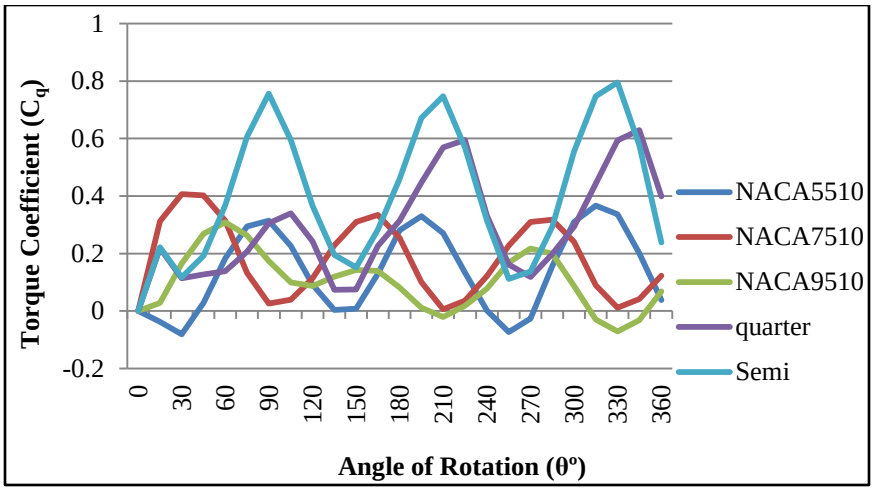

FIGURE 4-28: Torque Coefficient (C_q) vs. Angle of rotation (θ) for Three Blades Combined Effect at TSR 0.226 for Five Models

Figure 4.29 shows the torque variation with the change of Tip Speed Ratio. This point is recorded after 5 seconds of rotation. From this figure it can be concluded that with the increase of wind speed the corresponding values of torque increases. The optimum torque could not be found from this computational data. NACA5510 produces more torque than any other models at any point of wind speed. On the other hand Semi-circular rotor produces lowest torque.

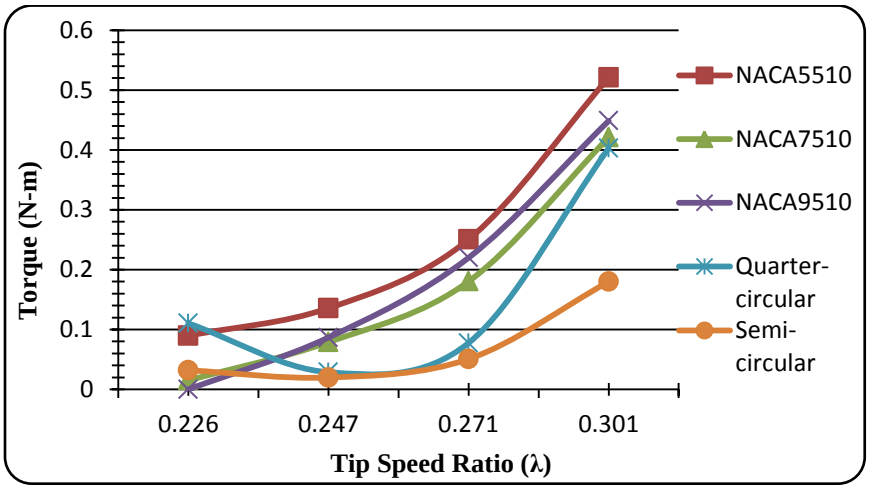

FIGURE 4-29: Torque (T) at 5sec. vs. Tip Speed Ratio (λ) for Different Blades

Figure 4-30 and 4-31 show the torque coefficient variation with the change of Tip Speed Ratio at the point after 5 seconds of rotation. The torque coefficient of Figure 4-30 is calculated from the torque and the other geometric parameters; Figure 4-31 is directly yielded from numerical solution. Torque coefficient shows the same trend of torque.

NACA5510 produces more torque than any other models at any point of wind speed. On the other hand Semi-circular rotor produces lowest torque. Though for circular shaped bladed rotors the torque coefficient is lowest around 0.250 TSR. From the curves, it is not evident that the increase of camber does not necessarily produce better torque coefficient.

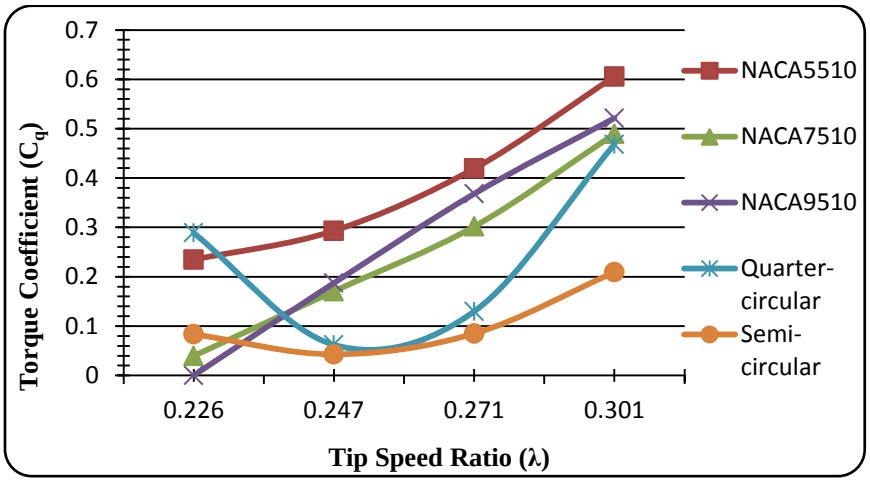

FIGURE 4-30: Calculated Torque Coefficient (C_q) at 5sec. vs. Tip Speed Ratio (λ) for Different Blades

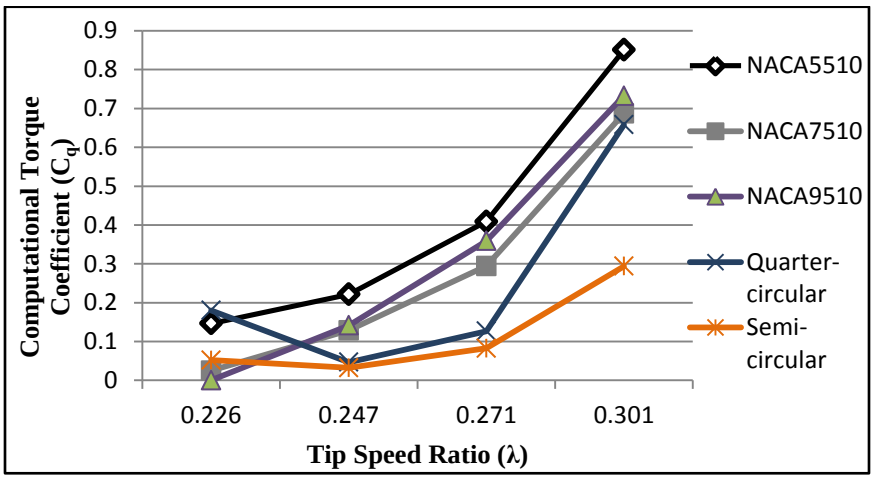

FIGURE 4-31: Computational Torque Coefficient (C_q) at 5sec. vs. Tip Speed Ratio (λ) for Different Blades

Figure 4-32 is the average of torque coefficients calculated at each 0.02 seconds for 5 seconds of rotation. For all the cases the minimum torque coefficient shows at 0.247 TSR except semicircular bladed rotor. The quarter-circular rotor shows the best result. NACA9510 showed better result among the airfoils.

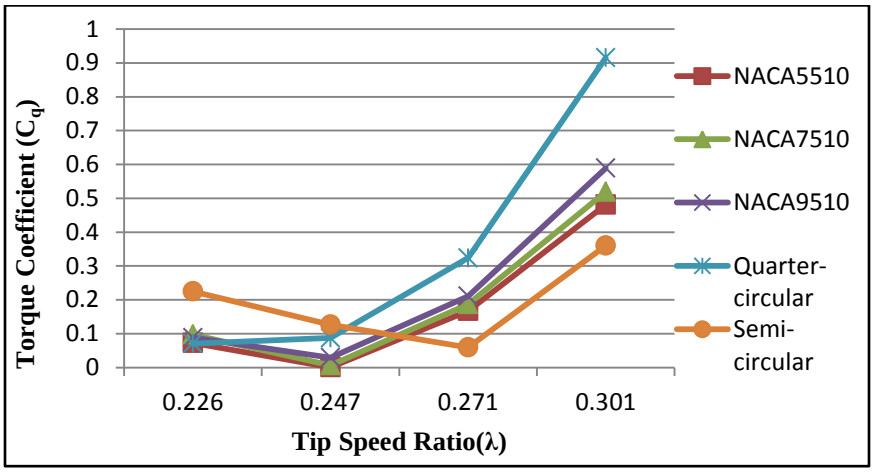

FIGURE 4-32: Averaged Torque Coefficient (C_q) vs. Tip Speed Ratio (λ) for Different Blades

Though figure 4-28 suggests that, semi-circular bladed rotor has better torque coefficient. But that shows the picture at second rotation. While figure 4-32 suggests quarter-circular bladed rotor has better torque coefficient which is the average of almost 100 rotations.

4.1.6 Power Coefficient

The power coefficient is shows the very same picture of torque coefficient. Figure 4-23 and 4-24 show the power coefficient variation with the change of Tip Speed Ratio. The first one is calculated from the power and the other geometric parameters; the second one is directly yielded from numerical solution multiplied by TSR. The increase of wind speed increases the corresponding values of power coefficient.

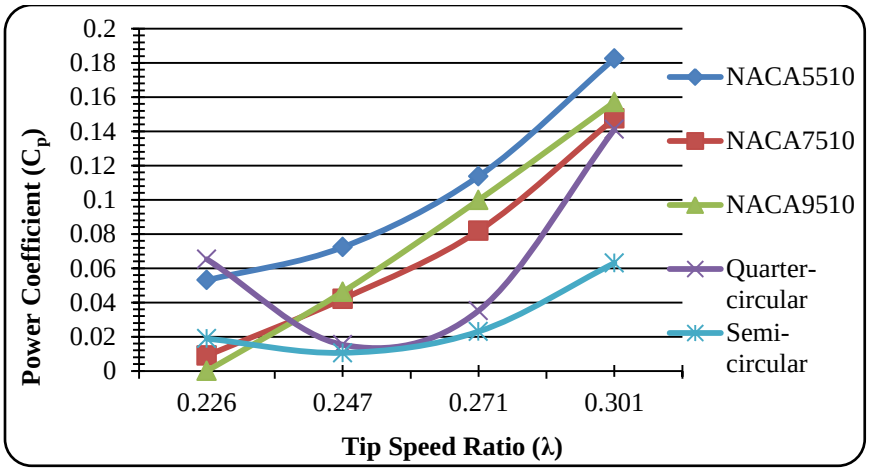

FIGURE 4-33: Calculated Power Coefficient (C_p) at 5sec. vs. Tip Speed Ratio (λ) for Different Blades

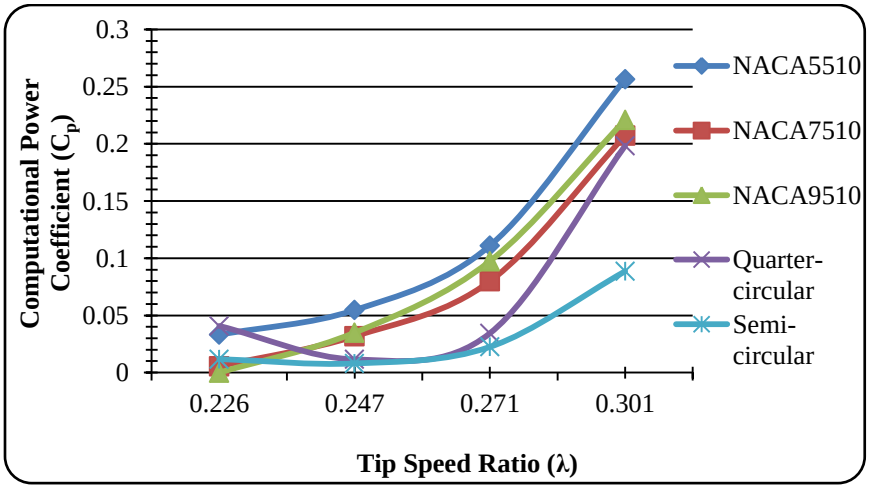

FIGURE 4-34: Computational Power Coefficient (C_p) at 5sec. vs. Tip Speed Ratio (λ) for Different Blades

NACA5510 shows better power coefficient than any other models at any point of wind speed and Semi-circular rotor produces the least. Both the circular shaped bladed rotors dropped the efficiency around 0.250 TSR. After NACA5510, NACA9510 produce more power.

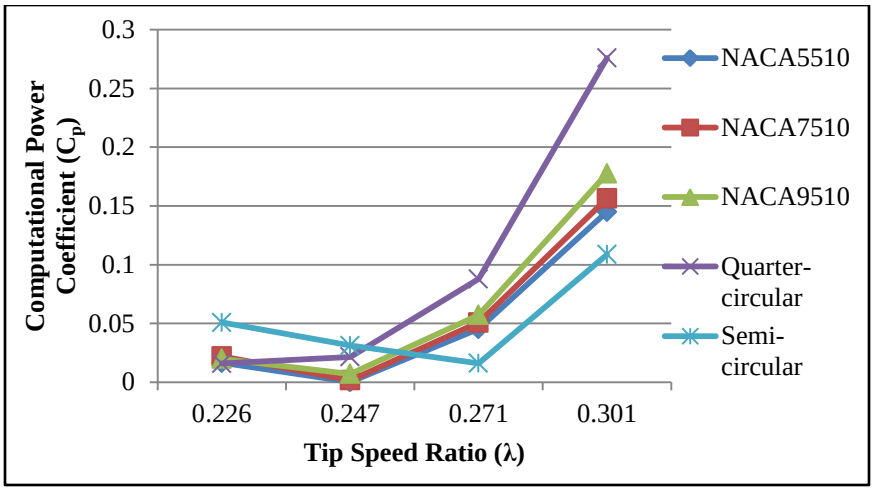

FIGURE 4-35: Averaged Power Coefficient (C_p) vs. Tip Speed Ratio (λ) for Different Blades

Figure 4-25 is the average Power coefficient. This is simply calculated from the average torque coefficient and TSR. Around 0.250 TSR all the models show least efficiency and then increases with the increase of TSR. Quarter circular shape produces better power coefficient.

4.2 Experimental Results

From the numerical solution, it was decided to create three models. They are NACA5510, NACA7510 and Semi-circular bladed rotor. The Models were tested at three different wind speeds.

4.2.1 Torque Coefficient

It is seen that Experimental result produces opposite of computational result. NACA 5510 produces lesser torque and semi-circular shape produces higher torque.

Calculating the torque and other parameters, semi-circular bladed rotor has very less increase of torque coefficient if the wind speed is increased. NACA 5510 also produces similar behavior. But the coefficient is lesser than semi-circular rotor. But NACA7510 produces a

good change of torque coefficient when the wind speed as well as TSR is increased. This behavior is plotted and figure 4-26 illustrates the behavior.

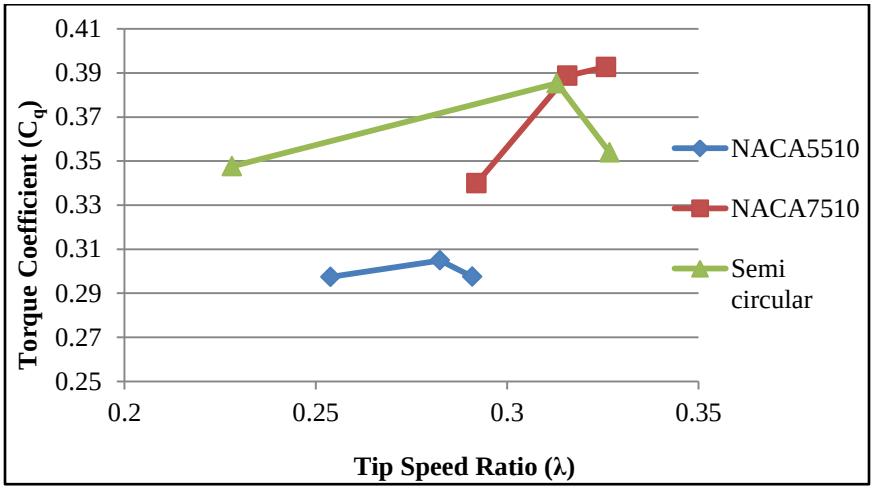

FIGURE 4-36: Torque Coefficient (C_q) vs. Tip Speed Ratio (λ) for Different Blades

4.2.2 Power Coefficient

Like torque coefficient, power coefficient also shows the similar picture. With the increase of Tip Speed Ratio, NACA7510 shows the best result among these three rotors. NACA5510 produces very low power coefficient.

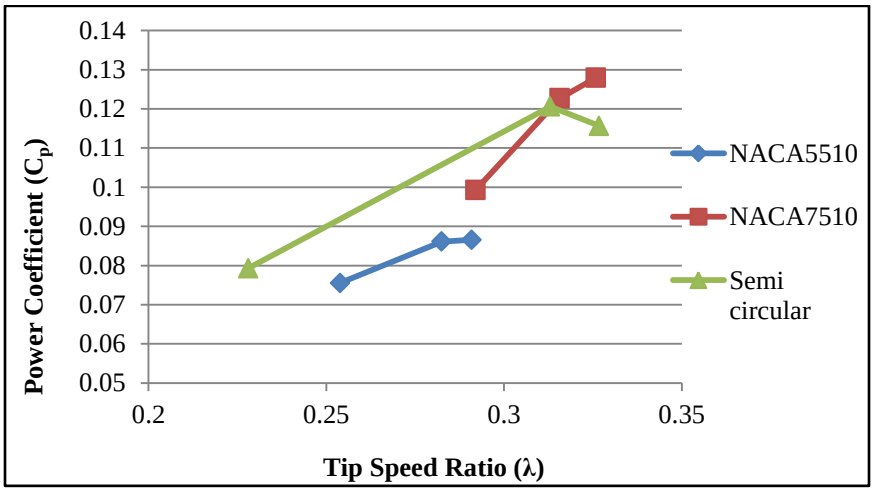

FIGURE 4-37: Power Coefficient (C_p) vs. Tip Speed Ratio (λ) for Different Blades

4.3 Comparison of Numerical and Experimental Power Coefficient

Figure 4-29 shows the comparison between numerically and experimentally calculated data. The experimental data has taken at some point of average data, so average computational data is also used here.

Figure 4-29 compares the torque coefficient characteristic of three blades at different TSR. Both computational and experimental data shows that NACA7510 profiled bladed rotor has a better result than others.

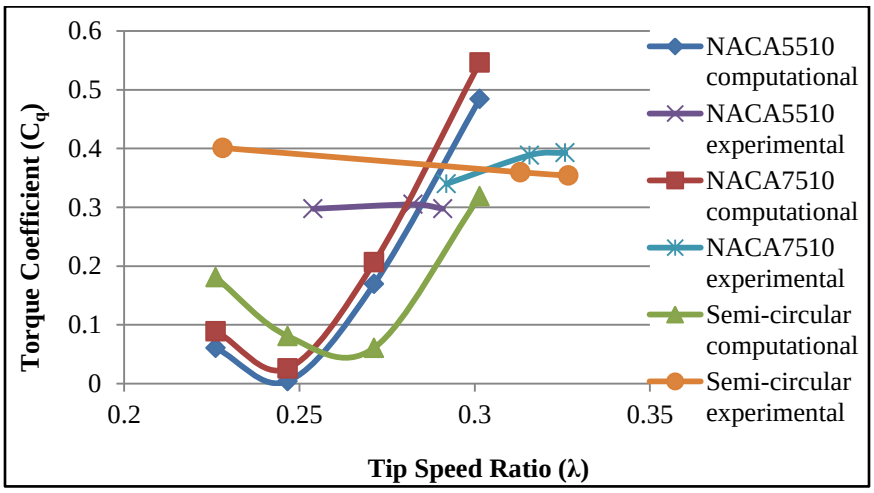

FIGURE 4-38: Torque Coefficient (C_q) vs. Tip Speed Ratio (λ) of Numerical and Experimental Result for NACA5510, NACA7510 and Semi-Circular Bladed Rotor

Power coefficient behaves the same way of torque coefficient here. NACA7510 characteristics are better than the other two rotors. Figure 4-30 shows the comparison of power coefficient (C_p) with the increase of TSR.

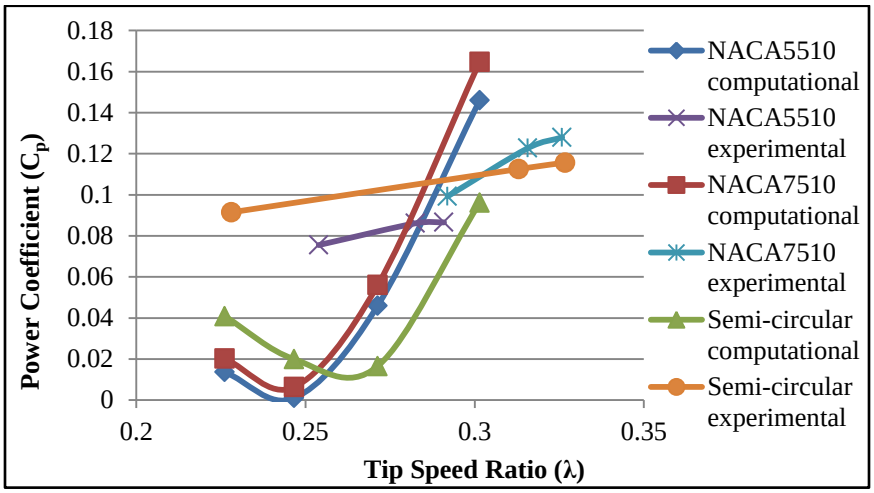

FIGURE 4-39: Power Coefficient (C_p) vs. Tip Speed Ratio (λ) of Numerical and Experimental Result for NACA5510, NACA7510 and Semi-Circular Bladed Rotor

CHAPTER 5

5 Conclusion and Recommendation

Five different three bladed Savonius type VAWT are designed and tested computationally. Then three of them are fabricated and experimentally investigated in front of a subsonic wind tunnel. All these experiments are tested at different wind speeds. Torque coefficient and Power coefficients are determined from both the methods and compared.

The experimental setup has some issues which could contribute some error during data acquisition.

5.1 Conclusion

After studying and analyzing all the yielded and calculated data, the conclusions are:

- NACA7510 provides the better torque coefficient than the other models. Though computationally NACA9510 provides slightly better torque coefficient.
- Power coefficient provides the similar result of Torque coefficient. The higher TSR the better power coefficient for all the models. NACA7510 shows overall better power coefficient. Computationally quarter circular bladed turbine and NACA 9510 provides better power coefficient.
- The torque and power coefficient decreases around TSR 0.250. Then with the increase of TSR, both the coefficient shows better result.
- From computational study, NACA5510 shows higher Drag Coefficient. With the increase of wind speed the drag force increases too.

- NACA7510 shows higher Lift coefficient. Around TSR 0.301 it seems that all lift coefficient reaches its optimum value as most of the curves seems to start declining.
- Camber of airfoil has definite impact on blade design. The change of camber percentage shows different characteristics.
- In most of the cases, airfoils showed better results than regular circular shaped turbines.

5.2 Recommendation

VAWT design can be improved by change of blade shape and number. The following recommendation can be made for more improvement of VAWT.

- Camber position, percentage and thickness percentage of airfoil can be changed for the different airfoil creation. This may show new behavior.
- To change the shape of blade, twisted blades from 15^0 to 90^0 can be examined.
- The airfoil blades can be used for Savonius and Darrieus type VAWT. In addition to that hybrid type VAWT can be created using both Savonius and Darrieus turbine.
- Changing the number of blade and stage can be another option which can also help to improve the performance.
- A better load system on the other side of dynamic transducer needs to be installed to get better dynamic torque data. Computer interface with the transducer can provide average data, which is not possible in current display system.
- The rotor needs to be properly vertically aligned, which means the shaft, torque transducer, load system and the overall frame should be aligned properly.
- To yield similar kind of result for different type of design, the geometry, weight and material of the rotor should be similar to get comparable data.

REFERENCE

Administration, Energy Information. "US Energy Information Administration." *Annual Energy Review.* 2013. www.eia.gov (accessed October 22, 2013).

Airfoil Tools. n.d. http://airfoiltools.com/airfoil/naca4digit (accessed September 24, 2013).

Armstrong, Shawn, Andrzej Fiedler, and Stephen Tullis. "Flow separation on a high Reynolds number, high solidity vertical axis wind turbine with straight and canted blades and canted blades with fences." *Renewable Energy* 41 (2012): 13-22.

Beri, H., and Y. Yao. "Effect of Camber Airfoil on Self Starting of Vertical Axis Wind Turbine." *Journal of Environmental Science and Technology* 4-3 (2011): 302-312.

Bishop, JDK, and Amartunga GAJ. "Evaluation of small wind turbines in distributed arrangement as sustainable wind energy oprtion for Barbados." *Energy Conversion and Management* 49 (2008): 1652-61.

Biswas, A., R. Gupta, and K.K. Sharma. "Experimental Investigation of Overlap and Blockage." *Wind Engineering* 31-5 (2007): 363–368.

Carrigan, Travis J., Brian H. Dennis, Zhen X. Han, and Bo P. Wang. "Aerodynamic Shape Optimization of a Vertical-AxisWind Turbine Using Differential Evolution." *International Scholarly Research Network ISRN Renewable Energy*, 2012.

Castelli, Marco Raciti, Andrea Dal Monte, Marino Quaresimin, and Ernesto Benini. "Numerical evaluation of aerodynamic and inertial contributions to Darrieus wind turbine blade deformation." *Renewable Energy* 51 (2013): 101-112.

Diaz, F., J. Gavalda, and J. Massons. "Drag and Lift coefficient of the savonius wind machine." *Journal of Wind Energy*, no. 15 (1991): 240-246.

Ghatage, Swapnil V., and Jyeshtharaj B. Joshi. "Optimisation of Vertical Axis Wind Turbine:CFD Simulations and Experimental Measurements." *The Canadian Journal of Chemical Engineering* 90 (2012): 1186-1201.

Ghosh, P., M. A. Kamoji, S. B. Kedare, and S. V. Prabhu. "Model Testing of Single and Three-stage Modified Savonius Rotors and Viability Study of Modified Savonius Pump Rotor Systems." *International Journal of Green Energy,* no. 6 (2009): 22–41.

Gupta, R., A. Biswas, and K.K. Sharma. "Comparative study of a three-bucket Savonius rotor with a combined three-bucket Savonius–three-bladed Darrieus rotor." *Renewable Energy* 33 (2008): 1974-1981.

Gupta, R., R. Das, R. Gautam, and S.S. Deka. "CFD Analysis of a Two bucket Savonius Rotor for Various Overlap Conditions." *ISESCO Journal of Science and Technology* 8-13 (May 2012): 67-74.

GWEC. *Global Wind Energy Council.* 2012. www.gwec.net (accessed October 20, 2014).

Hameed, M. Saqib, and S.Kamran Afaq. "Design and analysis of a straight bladed vertical axis wind turbine blade using analytical and numerical techniques." *Ocean Engineering* 57 (2012): 248-255.

Hau, E. *Wind Turbines: Fundamentals, Technologies, Application, Economics.* Springer. Germany, 2006.

Hayashi, T., Y. Li, Y. Hara, and Y. Suzuki. "Wind Tunnel Test on a Three Stage out phase Savonius Rotor." *Proceeding of European Wind Energy Conference and Exhibition.* London, England, 2004.

Hayashi, Tsutomu, Yan Li, and Yutaka Hara. "Wind Tunnel Test on a Different Phase Three-stage Savonius Rotor." *JSME International Journal* 48-1 (2005): 9-16.

Howell, Robert, Ning Qin, Jonathan Edwards, and Naveed Durrani. "Wind tunnel and numerical study of a small vertical axis wind turbine." *Renewable Energy* 35 (2010): 412-422.

Islam, M., DSK Ting, and A. Fartaj. "Aerodynamic models for Darrieus-type straight bladed vertical axis wind turbines." *Renewable and Sustainable Energy Reviews*, no. 12 (2008): 1087–109.

Kumbernuss, J., J. Chen, H.X. Yang, and L. Lu. "Investigation into the relationship of the overlap ratio and shift angle of double stage three bladed vertical axis wind turbine (VAWT)." *Journal of Wind Engineering and Industrial Aerodynamics*, no. 107 (2012): 57-75.

Launder, B. E., and D. B. Spalding. *Lectures in Mathematical Models of Turbulence.* Academic Press, 1972.

Manzoor, Hussain M, S Nawazish Mehdi, and P. Ram Reddy. "CFD Analysis of Low Speed Vertical Axis Wind." *International Journal of Applied Engineering Research* 3-1 (2008): 149–159.

Mohamed, MH, G Janiga, E. Pap, and D. Thevenin. "Optimal blade shape of a modified Savonius turbine using an obstacle shielding the returning blade." *Energy Conversion and Management*, no. 52 (2011): 236–42.

Morshed, Khandakar N. *Experimental and numerical investigations on aerodynamic characteristics of savonius wind turbine with various overlap ratios.* Statesboro: Georgia Southern University, 2010.

Morshed, Khandakar Niaz, Mosfequr Rahman, Gustavo Molina, and Mahbub Ahmed. "Wind tunnel testing and numerical simulation on aerodynamic performance of a three-

bladed Savonius wind turbine." *International Journal of Energy and Environmental Engineering* , April 2013: 4-18.

Price, Trevor J. *Oxford Dictionary of National Biography.* Oxford University Press, 2009.

Qasim, A.Y., R. Usubamatov, and Z.M. Zain. "Investagation and Design Impeller Type Vertical Axis Wind Turbine." *Australian Journal of Basic and Applied Sciences* 5(12) (2011): 121-126.

Ragheb, M. "Wind Energy Converters Concepts." 2012. https://netfiles.uiuc.edu/mragheb/www/NPRE%20475%20Wind%20Power%20Systems/Wind%20Energy%20Converters%20Concepts.pdf (accessed October 15, 2013).

Rahman, Mosfequr, Khandakar Morshed, and Mahbub K. Ahmed. "Numerical and wind tunnel investigation on aerodynamic coefficients of a three bladed savonius wind turbine with and without overlap between blades." *proceedings of the 2010 SAMPE fall technical conference.* Salt Lake City, Utah, USA, 2010.

Rahman, Mosfequr, Khandakar N. Morshed, and Ahsan Mian. "Aerodynamic Performance Analysis of Three Bladed Savonius Wind Turbine With Different Overlap Ratios and at Various Reynolds Number." *ASME 2010 International Mechanical Engineering Congress and Exposition, Vol: 5.* Vancouver, British Columbia, Canada, 2010. 1209-1219.

Rahman, Mosfequr, Khandakar Niaz Morshed, Jeffery Lewis, and Mark Fuller. "Experimental and numerical investigations on drag and torque characteristics of three-bladed savonius wind turbine." *proceedings of the ASME 2009 International Mechanical Engineering Congress & Exposition IMECE2009.* Lake Buena Vista, Florida, 2009. 85-94.

Reigler, H. "HAWT versus VAWT." 2003. http://www.victordanilochkin.org/research/turbine/papers/HAWT%20versus.pdf (accessed October 21, 2013).

REN21. "Renewables Global Status Report." 2014. www.ren21.net (accessed October 20, 2014).

Saha, U.K., and M. Jaya Rajkumar. "On the performance analysis of Savonius rotor with twisted blades." *Renewable Energy*, no. 31 (2006): 1776–1788.

Saha, U.K., S. Thotla, and D. Maity. "Optimum design configuration of Savonius rotor through wind tunnel experiments." *Journal of Wind Engineering and Industrial Aerodynamics*, no. 96 (2008): 1359– 1375.

Savonius, S. J. "The S rotor and its application." *Mechanical Engineering*, no. 53 (1931): 333-338.

Shepherd, D. G. "Historical Development of the windmill." *National Aeronautics and Space Administration office of management*, 1990.

Technica, Clean. *Clean Technica.* 2012. http://cleantechnica.com/wind-energy-facts/ (accessed October 20, 2014).

Wakui, Tetsuya, Yoshiaki Tanzawa, Takumi Hashizume, and Toshio Nagao. "Hybrid Configuration of Darrieus and Savonius Rotors for Stand-Alone Wind Turbine-Generator Systems." *Electrical Engineering in Japan* 150-4 (2005): 259–266.

Wulff, H.E. *The traditional crafts of Persia, their development, technology and influence on eastern and western civilization.* MIT press, 1966.